5G Communication with a Heterogeneous, Agile Mobile network in the Pyeongchang Winter Olympic competitioN

Grant agreement n. 723247

Deliverable D5.4
Ubiquitous sub meter accuracy positioning with Galileo and wireless network features

Date of Delivery:	31 May 2017
Editor:	Roc Maymo-Camps
Associate Editors:	
Authors:	Giuseppe Destino, Roc Maymo-Camps, Jani Saloranta, Benoit Vautherin
Dissemination Level:	PU
Security:	Public
Status:	Final
Version:	V1.0
File Name:	5GCHAMPION_D5.4_Final
Work Package:	WP5

	Title:	Deliverable D5.4: Ubiquitous sub meter accuracy positioning with Galileo and wireless network features
	Date: 31-05-17	**Status: Final**
	Security: PU	**Version: V1.0**

Abstract

This analyses and defines the 5G interoperability architectural framework integrating GNSS based technology. It also describes the methods to enable accurate positioning by using Galileo features and radio access with high carrier frequency, large antenna arrays and large bandwidth. Last, it specifies a test bed to demonstrate the performance in test cases representative of selected usage conditions.

Index terms

Positioning, 5G, GNSS, mmWave, Interoperability, Galileo

Contents

List of Acronyms

5G	5th Generation
ALASSO	Adaptive - LASSO
AOA	Angle Of Arrival
AOD	Angle Of Departure
BS	Base Station
DGNSS	Differential GNSS
DOP	Dilution Of Precision
GMM	Gaussian Mixture Model
GNSS	Global Navigation Satellite System
HPBW	Half Power BeamWidth
KPI	Key Performance Indicator
LASSO	Least Absolute Shrinkage and Selection Operator
mmWave	Millimeter Wave
MIMO	Multiple Input – Multiple Output
MS	Mobile Station
PoC	Proof-of-Concept
PPP	Precise Point Positioning
RTK	Real Time Kinematic
SIMO	Single Input – Multiple Output
SNR	Signal to Noise -Ratio
WRTK	Wide RTK
UE	User Equipment
ULA	Uniform Linear Array
URA	Uniform Rectangular Array

Table of Figures

1 Introduction

This document analyses and defines the 5G interoperability architectural framework integrating GNSS based technology.

Section 2 describes the methods to enable accurate positioning by using GNSS and Galileo features.

Section 3 describes the methods to enable accurate position with high carrier frequency, large antenna arrays and large bandwidth in the millimeter-wave (mmWave) band.

Section 4 defines a mixed GNSS/mmWave solution to cope with multipath in urban environments.

Section 5 specifies a test bed to assess the performance in representative test cases, along with the expected results.

2 GNSS positioning

This section describes how GNSS positioning can reach sub-meter accuracy. It starts by enumerating the positioning error sources, then it details the various techniques to get rid of these errors and to select the most suitable, and finally it provides the benefits brought by Galileo and 5G to GNSS positioning.

2.1 Positioning error sources

A GNSS receiver collects signals emitted by the GNSS satellites in its field of view. Then, with correlation techniques applied to these collected signals, the receiver estimates the ranges from the satellites. These ranges are called “pseudoranges” because they are affected by errors from various main sources. The table below lists these error sources along with their typical range error and highlight the ones that are mitigated with precise positioning techniques.

Error source	Origin	Typical range error	Mitigated with precise positioning techniques
Satellite clock	Even if the timing equipment of GNSS satellites is very precise and corrections are broadcasted in the GNSS signal, a small clock bias still remains.	1 m	✓
Satellite ephemeris	A GNSS satellite broadcast its own position within the signal, but with a limited accuracy.	1 m	✓
Ionosphere and troposphere	Signals from the GNSS frequency band are subject to delays in these atmospheric layers.	11 m	✓
Multipath	GNSS signals are reflected and delayed by ground infrastructures and vegetation.	2 m	✗
Receiver noise	Thermal noise generated by the receiver RF.	0.1 m	✗
Receiver clock	Mass-market receivers contain oscillators cheaper than the ones on-board the satellites. However, because all GNSS signals are similarly affected by the receiver clock, this error is easily mitigated by the receiver during the computation of the position.	N/A (removed by receiver)	N/A

2.2 Precise positioning techniques

In order to be able to reach a sub-metric positioning accuracy, these errors should be the most possible mitigated. Many techniques have been developed using an additional GNSS receiver, which is fixed and whose position has been precisely determined. This additional receiver (called a “reference station”) collects GNSS signals like a classical receiver, with which corrections can be applied since the exact position of the station is known. The errors that can be mitigated by these corrections are the following:

- Satellite clock
- Satellite ephemeris
- Ionosphere and troposphere

Multipath cannot be mitigated by a reference station since it is a very local source of error, and the receiver noise cannot be corrected either because it is specific to each GNSS receiver.

Thanks to all these corrections, sub-metric accuracy can be achieved if the receiver is placed in an open-sky environment that is not subject to strong multipath.

Two methods coexist to generate and provide corrections: Precise Point Positioning (PPP) and Differential GNSS (DGNSS). The following subsections will detail each of them and select the best one adapted to mass-market receivers.

2.2.1 Precise Point Positioning (PPP)

With the PPP method, reference stations are networked in order to combine their measurements and to compute very precise satellite clock, ephemeris, and optionally ionosphere/troposphere corrections. Any receiver, even far from a reference station, can benefit from these corrections with an Internet access, because the corrections calculated with the PPP method are independent from the position of the reference stations. The networks are either free of charge and managed by public organisations like the International GNSS Service (IGS), or commercial services requiring a subscription to be accessed (Novatel, NavCom…). shows the typical architecture of a user location based on PPP techniques.

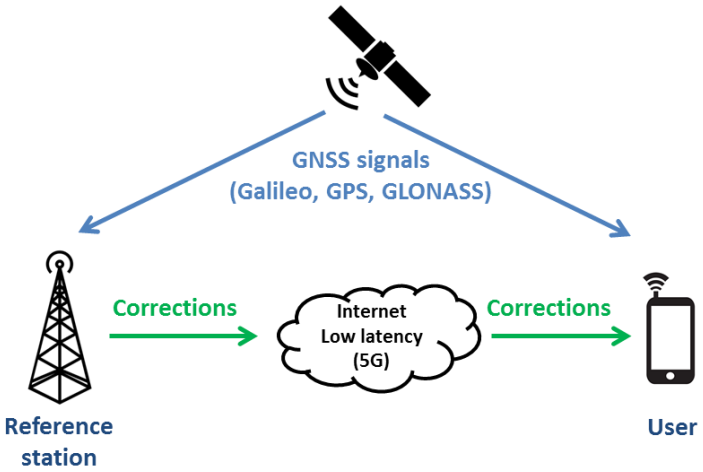

Figure 1: PPP technique

PPP data can also be provided by satellite link: this is planned for the future developments of Galileo [1]. However, the corrections would be transmitted on a separate sub-band (E6), which can only be received by multi-frequency receivers. Most of mass-market receivers are currently single-frequency because of cost matters, but affordable multi-frequency ones could appear in the following years.

In order to reach sub-meter accuracy, the receiver has to make carrier phase measurements instead of code phase measurements. Code phase processing uses the information of the satellite signal (the code) to compute the position, whereas carrier phase processing uses the radio signal (the carrier), which has a much higher frequency (see figure below).

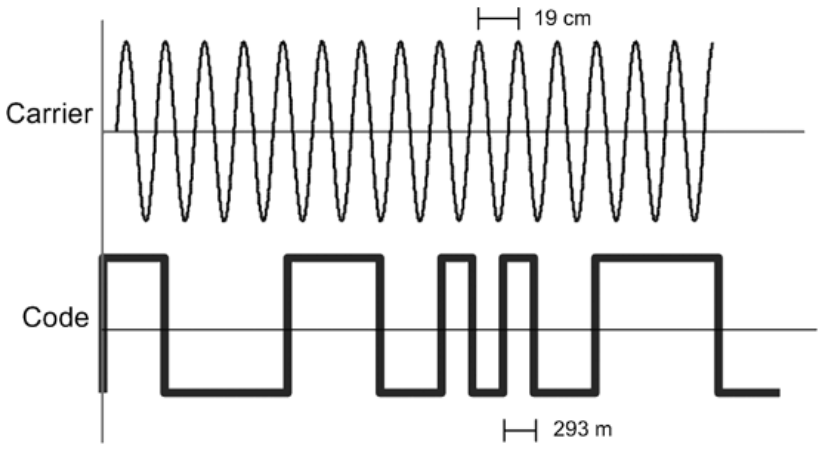

Figure 2: Illustration of the carrier and the code of a GNSS signal

However, the number of phase cycles for the carrier between the satellite and the receiver, which is unknown (contrary to the number of code cycles), has to be determined by the receiver: this is called “ambiguity resolution”. The ability to resolve ambiguity depends on the signal C/N0 and on multipath: an open-sky environment is clearly more adapted than urban environment where multipath is omnipresent. Because of this ambiguity resolution step, PPP will have a long convergence time, but sub-metric accuracy can be achieved in minutes if ionospheric corrections are applied. The figures below**Erreur ! Source du renvoi introuvable.Erreur ! Source du renvoi introuvable.Erreur ! Source du renvoi introuvable.Erreur ! Source du renvoi introuvable.** compare the accuracy of single positioning with PPP, and show the rapid sub-metric convergence of PPP with ionospheric corrections..

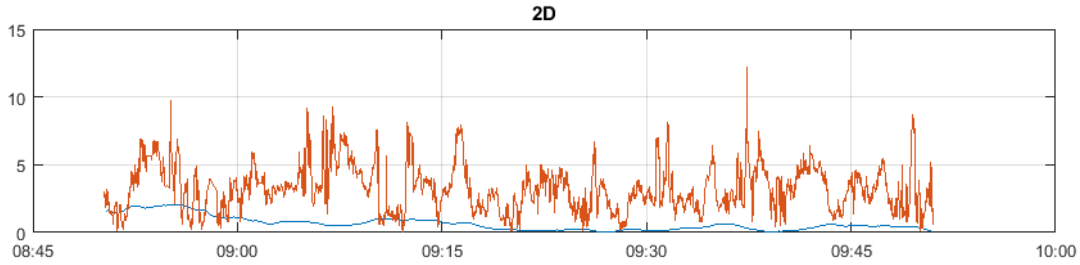

Figure 3 : Single positioning vs PPP accuracy (m)

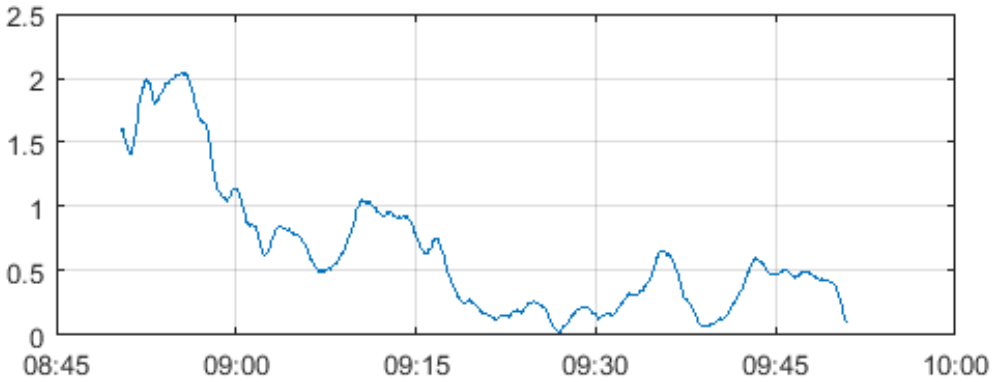

Figure 4: PPP convergence with ionospheric corrections (m)

2.2.2 Differential GNSS (DGNSS)

Contrary to PPP, reference stations in DGNSS are independent and do not communicate with each other. Instead, the reference station broadcasts its pseudorange measurements, which are used by the user’s receiver to mitigate clock, ephemeris troposphere and ionosphere errors. The corrections apply only in the vicinity of the station: the positioning

accuracy of the DGNSS method can be less than 1m if the baseline (distance from the receiver to the reference station) is less than a few tens of kilometres.

There are two main DGNSS methods: standard and Real Time Kinematic (RTK), depending on the type of measurement that is used.

With standard DGNSS, the user's receiver computes its position with algorithms based on code measurements of the GNSS signals from the reference station and the user itself (Figure 5, left), contrary to RTK algorithms, which are based on carrier phase measurements (Figure 5, right).

Like the PPP technique (see above), RTK leads to a better accuracy because of these carrier phase measurements, but it is as well subject to the ambiguity resolution issue. However, the ambiguity will be resolved much faster than for PPP thanks to the phase measurements of the reference station that are transmitted to the user's receiver.

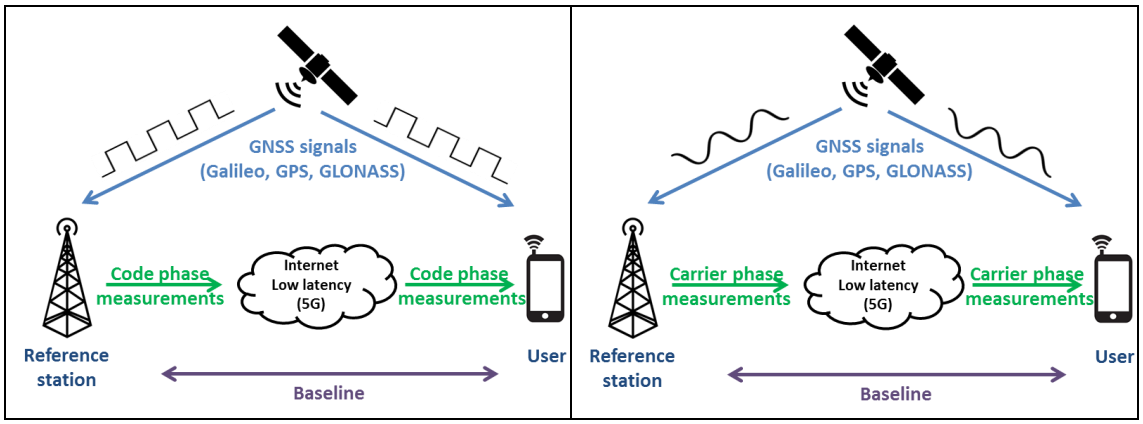

Figure 5: Standard DGNSS (left) and RTK (right)

2.2.3 PPP, standard DGNSS and RTK trade-off

The table below shows the main characteristics of the three methods:

	PPP	Standard DGNSS	RTK
Accuracy	< 1m	~ 1m	< 1m
Convergence	> 5mn	< 1mn	< 1mn
Availability	In open-sky areas	In open-sky areas	In open-sky areas
Baseline	Infinite	< 50 km	< 50 km
Bandwidth	< 10 kb/s	< 10 kb/s	< 10 kb/s
Service cost	Free	Free	Free

All the three GNSS positioning methods can be used free of charge and require a very low data rate. Standard DGNSS can hardly reach a sub-meter accuracy. The RTK method is very

accurate and has a short convergence time, but reference stations should form a costly and dense network because the range from the user to the reference station should not exceed 50 km. The long convergence time of the PPP method makes it currently unsuitable for most usages, like pedestrian or road navigation, but ionospheric errors can be mitigated by a stream of corrections or a dual-frequency receiver, and techniques are under investigation to reduce the convergence time [4].

PPP is therefore the most promising technology for the coming years: that is why it has been selected for demonstration in the scope of this project.

2.3 Galileo: a great improvement for GNSS localisation

Before 2011, only GPS and GLONASS satellites were able to provide a positioning service above Europe. The on-going deployment of Galileo, the European GNSS constellation, and its support by recent mobile terminals, opens new perspectives for a more accurate and ubiquitous GNSS localisation for a wide range of users. Indeed, Galileo benefits from a number of technical improvements and new features compared to GPS and GLONASS systems. To name main benefits:

Better availability and accuracy. 31 GPS and 24 GLONASS satellites are currently in operation. As of today, Galileo add 11 more GNSS satellites, and the full operational constellation will be composed of 24 operational spacecraft.

Generally speaking, more satellites available to the user for localisation translates to a better positioning accuracy and a better availability of the positioning service, especially in zones with a limited sky view. This is shown by the figures below: to simulate an urban environment, the coordinates of Toulouse city have been set and satellites below 40° of elevation have been masked. With GPS and GLONASS, there are some time slots where less than 4 satellites are visible, which makes the localisation impossible. For instance, like shown in Figure 6: only 2 GPS and 1 GLONASS are available at time 15:10, but with Galileo two more satellites are added (yellow line) and localisation is possible.

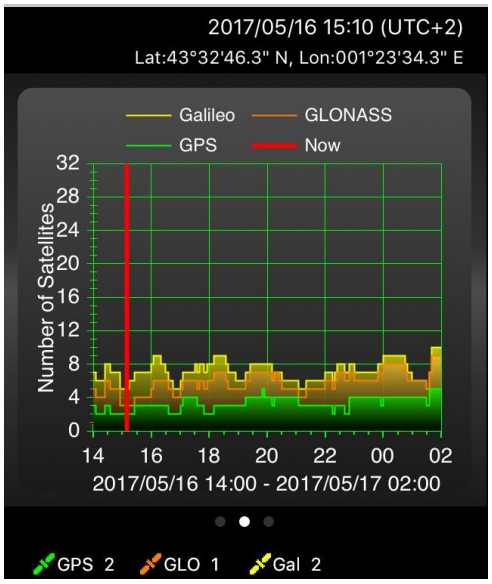

Figure 6: Number of visible satellites with a 40° mask

The dilution of precision (DOP) value reflects the effect of satellite geometry on the positioning accuracy (Langley, 1999). A high DOP means that the satellites used for positioning are closed to each other, limiting the accuracy (Figure 7).

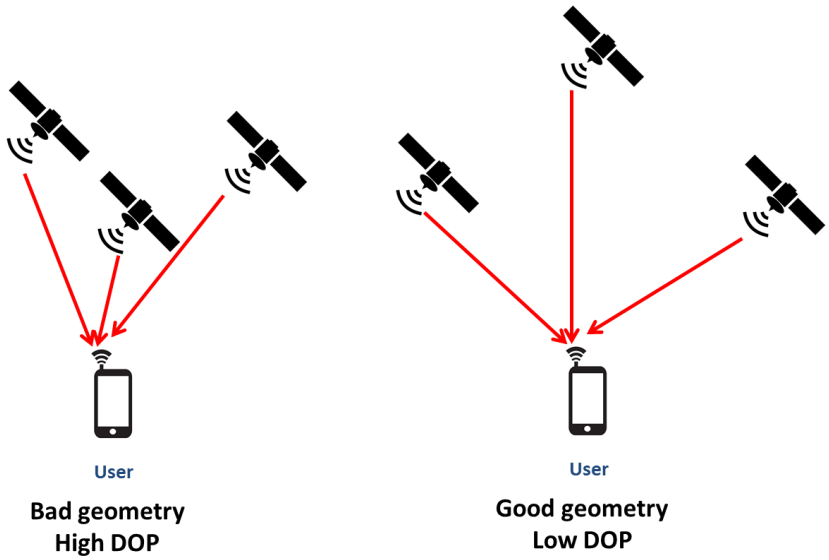

Figure 7: Satellite geometry and DOP

The introduction of the Galileo constellation also significantly improves the positioning accuracy in zones with a limited field of view by reducing the DOP, as shown in Figure 8: the DOP drops from 13.6 to 7.5 when Galileo is added.

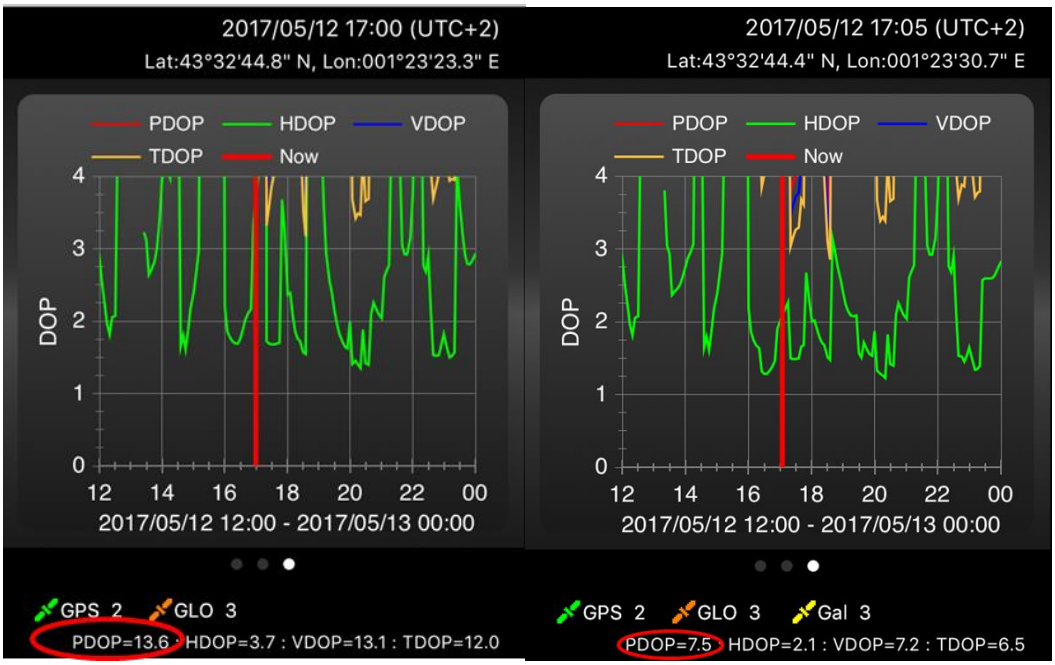

Figure 8: DOP with and without Galileo, 40° mask

Robustness to multipath. Galileo signals have been designed to be more resistant to multipath propagation, as shown by the theoretical multipath envelope in Figure 9: the code phase error is much lower for Galileo than for GPS.

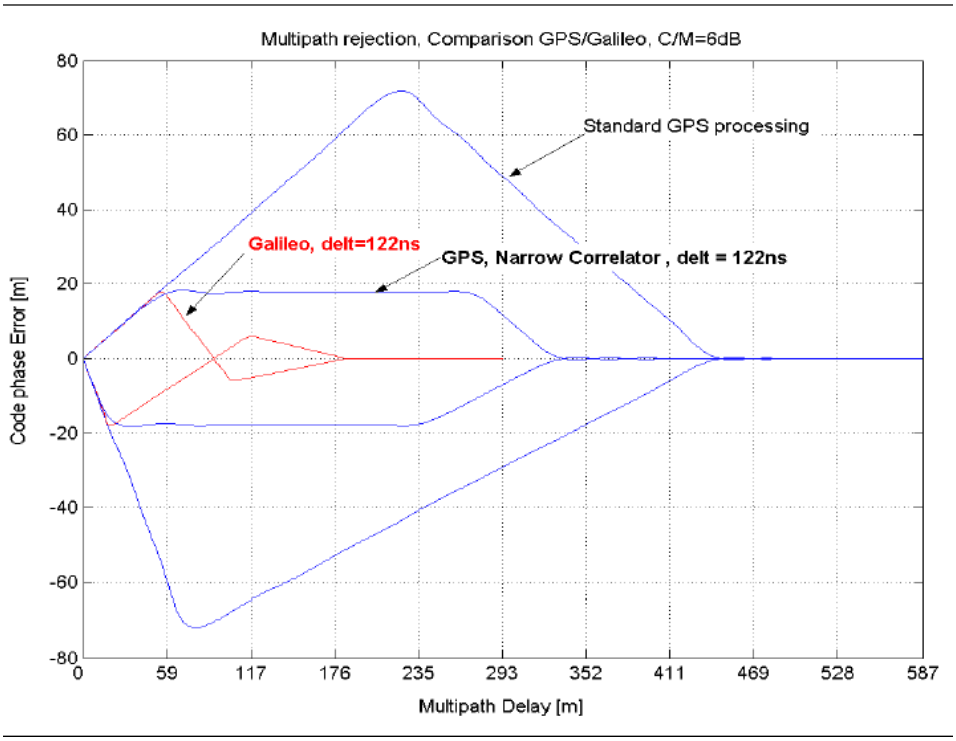

Figure 9: Code phase error in presence of multipath

This is confirmed by measurements on the GNSS reference station in Oulu that will be used in the scope of this project:

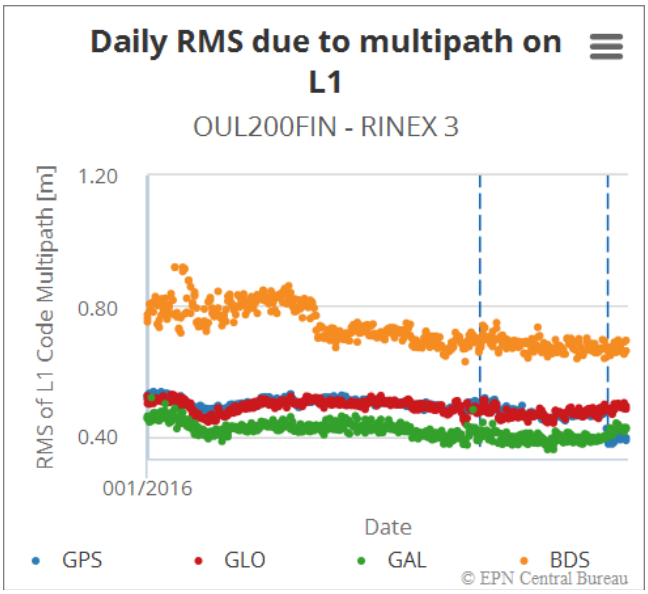

Figure 10: RMS error due to multipath for various GNSS constellations

Better Earth coverage. The inclination of Galileo orbital planes was chosen to provide a better coverage at high latitudes, especially for operation over northern Europe, an area poorly covered by GPS.

2.4 5G: the ideal channel to transfer reference station data

Ephemeris are coded and transmitted by the satellites in their navigation signal, but with a very low data rate: a receiver doing a “cold start” should wait up to two minutes to get the position of all visible satellites. To speed up this process, mass-market receivers like smartphones usually download these ephemeris from the Internet: this is called A-GNSS.

With the 5G technology, according to [3], several hundreds of thousands of users could be simultaneously connected to the same 5G station. This increased capacity compared to 3G or 4G networks could be used to disseminate PPP corrections from nearby reference stations to all users at the same time and with a very short latency. The 5G channel would not be overloaded by this PPP link because it requires a data rate of only a few kb/s.

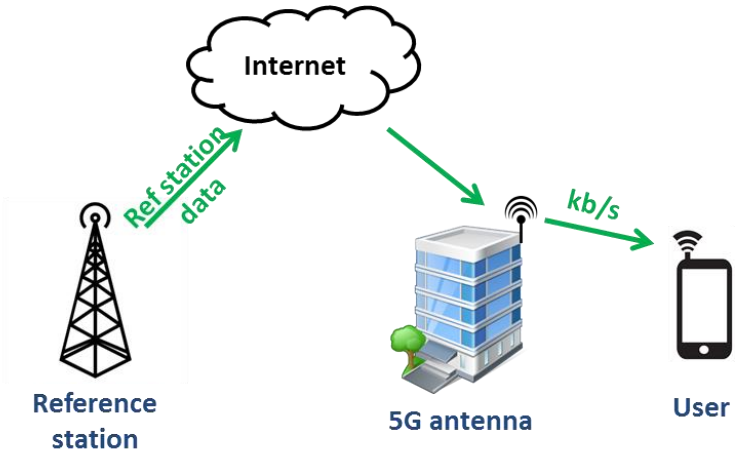

Figure 11: Use of 5G network for reference station data

3 mmWave positioning

3.1 Concept

In this Section, we introduce the concept of millimeter-wave (mmWave) technology for positioning application for future (5G) radio systems and discuss about the tunable parameters on those.

The mmWave technology[1] is considered as one of the key properties of the next generation (5G) communication networks. The communication system based on mmWave can take an advantage of two important properties introduced by the mmWaves: First, it allows high data rate and secondly the utilization of large antennas (a large number of elements on antenna array) for massive multiple-input-multiple-output (MIMO) system [P2, P3]. Thus one important feature, beamforming, can be utilized via the large antenna arrays [P4].

Rest of the Section is organized as follows, first in Section 3.2, we describe the system model, namely channel model and antenna model assumed at receiver and transmitter, and furthermore describe the beamtraining method. Then in Section 3.3, we describe the positioning method given the channel estimation results. Finally, in Section 3.4 we provided a performance analysis of position and rotation estimation of 5G mmWave system.

3.2 System model

3.2.1 System overview

The proposed mmWave positioning technique is based on the single basestation (BS) system, and thus it consists only one receiver and one transmitter radio (in one mobile user case). The technique can be extended to account multiple BS.

Each radio part is described in more detail in 5GChampion documents [D2.1, D3.5, D3.6]] and publication [P14], namely components:

- 5G antenna system (including antenna array and computing unit) which provides the beam information to be used to calculate the link-based position at the server. Antenna array used in the Proof-of-Concept (PoC) platform are described in more detail [D3.2, D3.3];
- The server that provides the beam information (angular information) upon user request.

In the following, we will introduce shorty the mmWave MIMO radio channel, antenna model, and beamforming principle to utilized in the proposed algorithm.

3.2.2 mmWave MIMO communication model

Consider a mmWave single-user MIMO wireless system. The location of the transmitter, base-station (BS), and the receiver, user equipment (UE) (or mobile-station (MS)), are denoted by $\mathbf{q} \in \mathbb{R}^2$ and $\mathbf{p} \in \mathbb{R}^2$ in the given coordinate system, respectively. We assume that the location of BS **q** is known, whereas the location of MS **p** is not. Furthermore, the rotation of BS is assumed to be 0° (related to the common reference system) while MS has an unknown rotation denoted by α. Thus, BS and MS have different orientation with respect to a

[1] A radio frequency band of 30 – 300 GHz via exact definition. Although relaxed definition are e.g. from 23 – 32 GHz bands [P1].

common reference system. The line-of-sight (LOS) view from BS to MS is denoted by φ, and from MS to BS (accounting rotation) by θ (note that rotation α is related through α = π - θ + φ). The model is illustrated in Figure 12 with 2D antenna array of BS and MS positioned at afore mentioned location **p** and **q**, respectively. MS has unknown orientation α relative to BS.

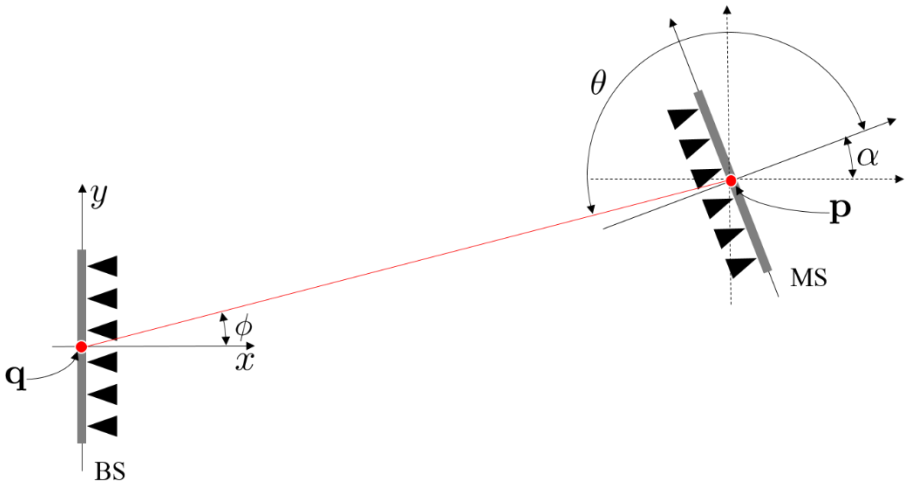

Figure 12: Geometry of the MIMO communication

We consider that both transmitter and receiver are equipped with uniform rectangular array (URA) with $M_y \times M_z$ and $N_y \times N_z$ isotropic elements on the BS side and MS side, respectively. Extension to 3D antenna array is straightforward, but to easen the notation as well as to match the antenna types that will be used in 5GCHAMPION PoC demonstration platform, the model is described with 2D antennas. An example of URA antenna with $M_y = 8$ and $M_z = 10$ is illustrated in Figure 13.

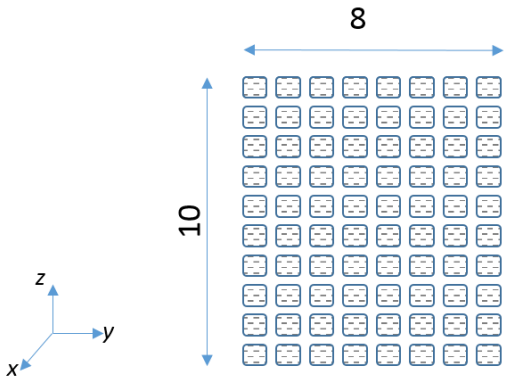

Figure 13: Uniform rectangular array (URA) antenna model

The URA antenna array coefficient for given path azimuth θ and elevation ϕ matrix **A** is given as

$$a(u) = \left[e^{-j2\pi u_2(m-1)}\right]|_{m=1,\ldots,M_y} \otimes \left[e^{-j2\pi u_3(n-1)}\right]|_{n=1,\ldots,M_y},$$

where

$$u = [0, |\cos\theta \sin\phi|, |\sin\theta|]$$

Furthermore, we assume in the following antenna element separation d = λ/2 element separation, where λ is the carrier wavelength. Antenna implementation technologies are discussed on detail 5GCHAMPION deliverable D3.1.

3.2.3 Channel model

We assume a channel model, where radio paths can be presented as a set of clustered paths. This *sparsity* induced channel model is illustrated in Figure 14, where first 2 dimensions are depicted (on the left side), namely the received side angular domain and time delay component, and then two more dimensions are depicted (on the right side) for one cluster on those domains, namely transmitter side angular domain and Doppler domain. [P5]

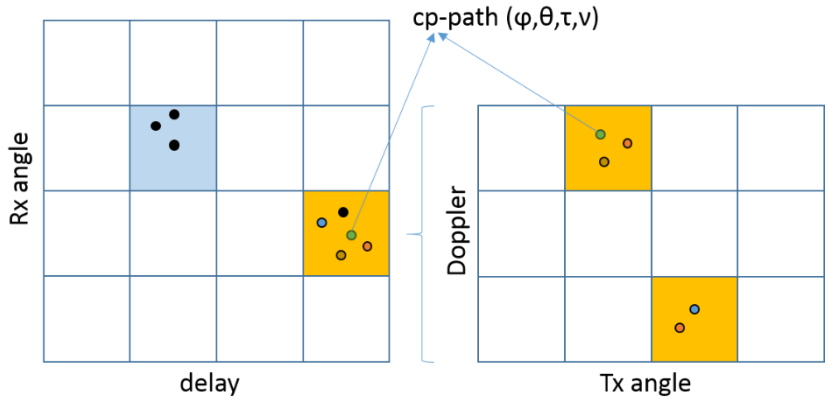

Figure 14: Sparse channel representation as a 4-dim tensor

Now, the full-dimensional channel model can be presented as 4-dimensional tensor:

$$\underbrace{\mathcal{H}}_{4D-tensor} = \sum_{c=1}^{C}\sum_{p=1}^{P_c} b_{cp}\, \mathbf{v}_r \underbrace{\left(\frac{\mathbf{P}_r^T \mathbf{u}_{r,cp}}{\lambda}; M\right)}_{\text{RX spatial frequency}} \circ \mathbf{v}_t \underbrace{\left(\frac{\mathbf{P}_t^T \mathbf{u}_{t,cp}}{\lambda}; N\right)^*}_{\text{TX spatial frequency}} \circ \mathbf{v}_f \underbrace{\left(\frac{\tau_{cp} W}{N_{\text{FFT}}}; N_{\text{FFT}}\right)}_{\text{DFT-frequency}} \circ \mathbf{v}_d \underbrace{\left(\frac{\nu_{cp} T_0}{T}; M_d\right)}_{\text{Doppler frequency}}$$

where each tensor-component is sum of P_c paths in total of C clusters, where each path is given as function of radio path coefficient b_{cp}, array factors $\boldsymbol{v_r}$ and $\boldsymbol{v_t}$, for receiver and transmitter side, respectively, and Doppler frequency vector. Note that the Rx and Tx spatial frequency components are function of transmitter and receiver position $\mathbf{P_r}$ and $\mathbf{P_t}$, and M, N are 'total' number of antenna elements.

Then as a mmWave channel can be seen via "quasi"-optical propagation properties [P6], we assume a single-path MIMO channel **H** given by

$$\mathbf{H}(\theta,\phi) = h a_R(\theta) a_T(\phi), \tag{1}$$

where *h* is the dominant channel coefficient, and $a_R(\theta)$, $a_T(\phi)$ are the transmit and receive array response vectors for the angle-of-departure (AoD) ϕ and angle-of-arrival (AoA) θ.

Then the received signal *y* can be written as a function of angular domain or as a function of relative position vector **p** as

$$\begin{aligned} y(t) &= \sqrt{P_{tx}} h \mathbf{w}^H \mathbf{a}_M(\theta) \mathbf{a}_N^H(\phi) \mathbf{f} x(t-\tau) + \mathbf{w}^H \mathbf{n}(t) \\ &= \sqrt{P_{tx}} h \mathbf{w}^H \ddot{\mathbf{a}}_M(\mathbf{p},\alpha) \ddot{\mathbf{a}}_N^H(\mathbf{p},\alpha) \mathbf{f} x(t-g(\mathbf{p},\alpha)) + \mathbf{w}^H \mathbf{n}(t) \end{aligned} \tag{2}$$

where P_{tx} is transmitted power; **f** and **w** are the transmiter and receiver side unit-norm beamforming vectors, which are generated from the given codebooks (the codebook sizes denoted by *M* and *N* are based on the size of antenna array on BS and UE size); **n** is additive white Gaussian (AWGN) noise with power spectral density (PSD) N_0; $\tau = \|\mathbf{q}-\mathbf{p}\|/c$ is time-delay of the LOS path; and the MS location defines the parameters on second form

$$\begin{bmatrix} p^x \\ p^y \\ \alpha \end{bmatrix} = \begin{bmatrix} q^x + c\tau\cos(\phi) \\ q^y + c\tau\sin(\phi) \\ \pi + \phi - \theta \end{bmatrix} \tag{3}$$

Beamforming procedure and codebooks associated to that, are discussed in the next Section.

3.2.4 Beamforming

In this Section, we present two beamforming strategies, namely an exhaustive and a hierarchical strategies. Exhaustive strategy is used as a solution with *less risks*, keeping mind on the real life demonstration and tests, as hierarchical strategy is used as a more realistic from the point of view of real life performance requirements. The implementation and integration of Beamforming technique is reported at [D3.4], hardware components are given in detail at [D3.6]. Our study of the trade-off between positioning and data rate is reported on [D3.5].

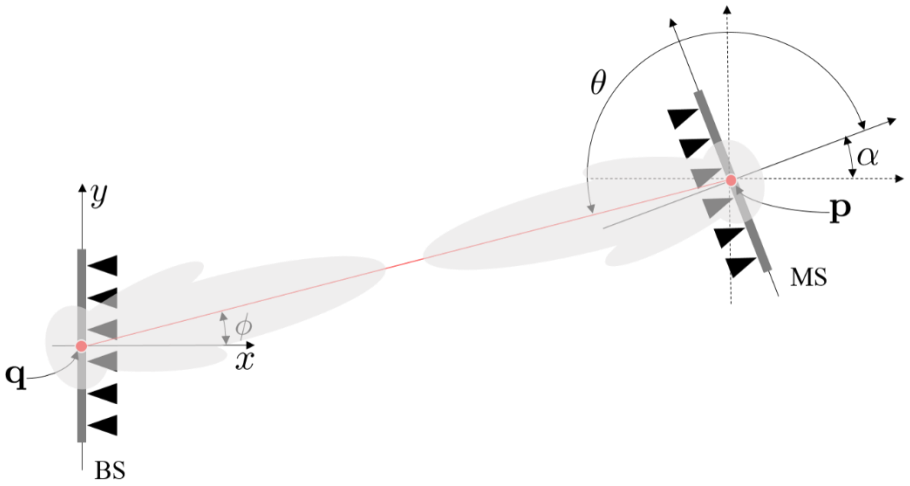

Figure 15: Illustration of the beamforming concept

Figure 15 illustrates the concept of beamforming, where perfect beamforming results to the correctly aligned mainlobes of the beams from BS and MS and vice-versa.

3.2.5 Positioning Protocol

In this Section, we describe the proposed 5G positioning protocol. Communication occurs over frames of duration T_f of which a time T_t is devoted to beamtraining, *i.e.*, determining the best **w** and **f**. Then the remainder $T_d = T_f - T_t$ is used for data transmission. The frame structure is illustrated in Figure 16. The frame allocation between the data-rate and beamtraining is result in a trade-off: More time is given for the beamtraining process, less time there is for the data transmission within a slot. Then on the other hand, more time there is for beamtraining, better the beam alignment will be, which in will improve the achieved data rate. This trade-off is investigated and reported in [D3.4].

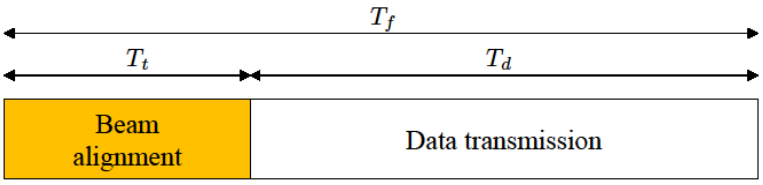

Figure 16: Training and Data transmission time trade-off

3.2.6 Beamforming and location

In this Section we describe an exhaustive and a hierarchical beamtraining strategies. For simplicity, we assume that the codebook dictionaries at the receiver side and the transmitter side are equal.

3.2.6.1 Beamforming Exhaustive Search

In the exhaustive beamtraining strategy, both, receiver side and transmitter side codebooks are orthogonal, for instance, specific columns from the Discrete Fourier Transform (DFT) of *N*-size matrix, where *N* is number of antenna elements. The example of orthogonal beams derived from the DFT codebook is illustrated in Figure 18. The beamtraining mechanism consists of sounding all possible transmit-receiving pairs of beams and, for each pair, measure the receiving power. After all beam-pairs have been scanned, then the receiver informs the transmitter about the beam-pair index corresponding to the maximum receiving power. The beamtraining allocation is illustrated in Figure 17.

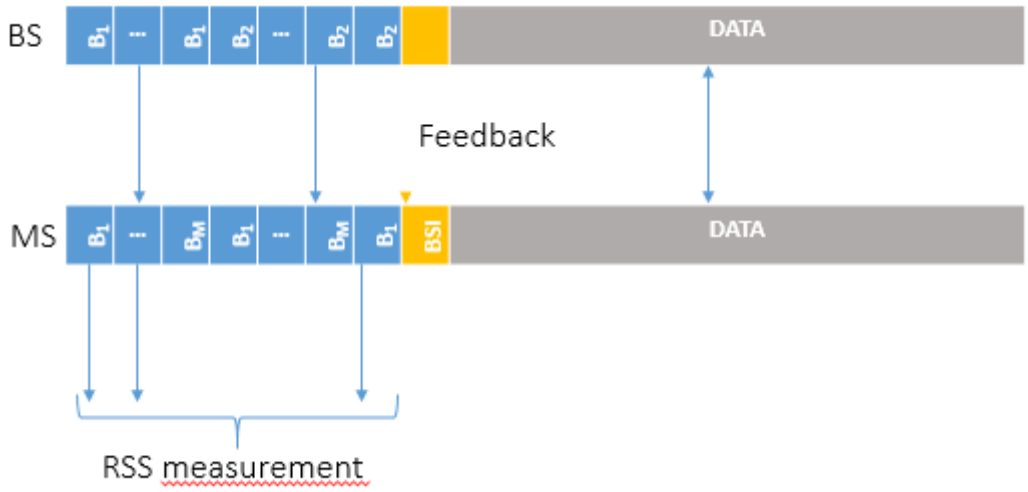

Figure 17: Exhaustive search beamtraining allocation on a radio frame

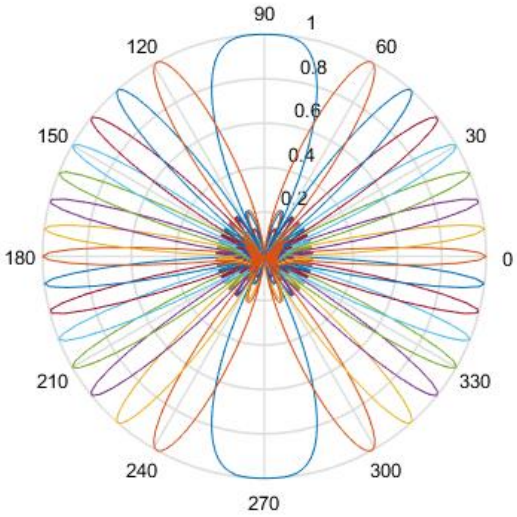

Figure 18: Illustration of the beams from DFT codebook with 16 beams

3.2.6.2 Beamforming: Hierarchical Search

In the hierarchical beamtraining strategy, receiver and transmitter side codebooks are generated based on a *nested partitioning* of the angular domain. In other words, we start by partitioning the whole angular domain, e.g., $[-\pi/2, \pi/2]$, in K bins. For each bin, we design a beamformer such that the half power beamwidth (HPBW) coincides with the upper and lower bounds of the bin. Next, each angular bin is further partitioned in K bins and, a new set of beamformer is constructed. It results, that $L = \lceil log_K N \rceil$ partitioning (also referred to as level) are performed and at for the l-level, K_l beamformer vectors are defined. The example of codebooks for different levels of K = 0,1,2,3 is illustrated in Figure 20.

The hierarchical search strategy seeking for the link with the highest SNR is performed as divide-and-conquer algorithm. Namely, base station (BS) and mobile station (MS) start with an exhaustive search mechanism using the K beamformers of level-1. Based upon the measured receiving power, a new exhaustive search with the K beamformers of level-2 is performed. This procedure iterates until beamformers of level-L are utilized. The beamtraining allocation of this strategy is illustrated in Figure 19.

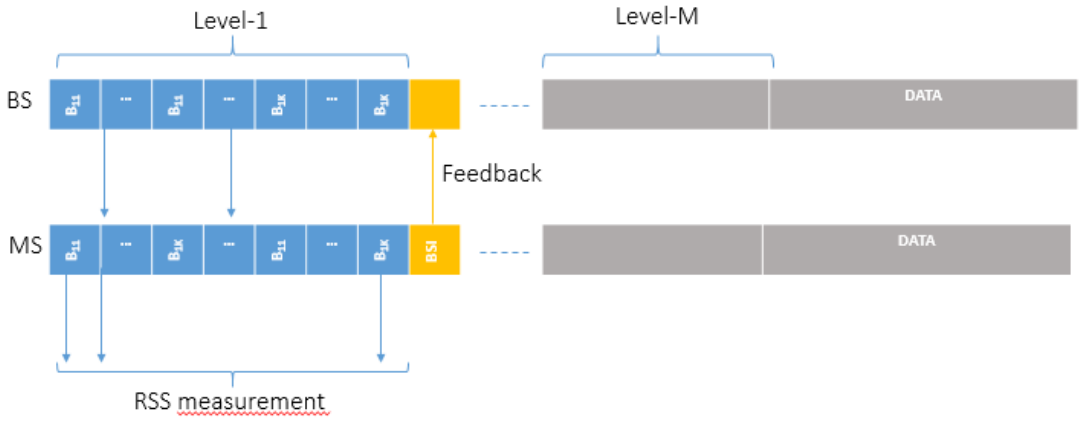

Figure 19: Hierarchical search beamtraining allocation on a radio frame

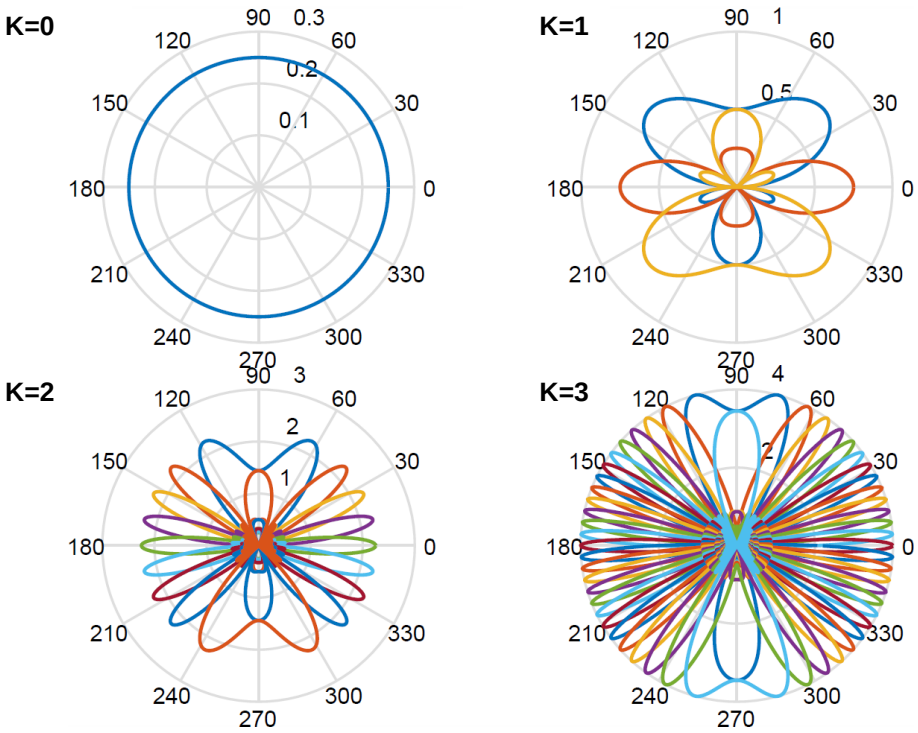

Figure 20: Illustration of the beams from the proposed hierarchical codebook design

3.3 From Channel Estimation to Position Estimate

In this Section, we describe a technique to derive position estimate from the channel estimation parameters. The key technique to employed is a channel estimation from the set of dictionary elements, *atoms*, via updating, *i.e.*, adapting the set of atoms to the existing

radio channel during the estimation process. To ease the formulation, we consider a MISO link alternative to the MIMO in following derivation.

First, let us consider the user location **x** as a function of location of BS denoted by **b**, Line-of-Sight (LOS) path-delay τ, and azimuth $\bar{\phi}$ and elevation $\bar{\theta}$ angle of arrival corresponding the LOS path

$$\mathbf{x} = \mathbf{b} + r\left[\cos(\bar{\phi})\cos(\bar{\theta}), \sin(\bar{\phi})\cos(\bar{\theta}), \sin(\bar{\theta})\right]^{\mathrm{T}},$$

where *r* is path-delay converted to the range estimate via *r* = c τ, given the speed-of-light constant *c*. Now we can formulate the position estimation problem on the received signal **Y** as

$$(\hat{\mathbf{x}}, \hat{\mathbf{\Delta}}, \hat{\boldsymbol{\beta}}) = \min_{\boldsymbol{\beta}\in\mathbb{C}^L, \mathbf{x}\in\mathbb{R}^3, \mathbf{\Delta}\in\mathbb{R}^{3\times L}} \|\mathbf{Y} - \mathbf{W}^{\mathrm{H}}\mathbf{A}^{\mathrm{H}}\mathcal{H}(\mathbf{x}, \mathbf{\Delta})\mathbf{X}\|_2^2,$$

where the symbol **Δ** accounts estimation error from true **x** to the estimated $\hat{\mathbf{x}} = \mathbf{x} + \mathbf{\Delta}$, β is channel coefficient, and L is the number of components each channel vector **h** is decomposed. The difficulties to solve the minimization problem is discussed in [P7], where the authors propose an indirect approach, in which the channel parametrization given in [P6], [P9] is exploited to generate a set of position estimate images and from where the final estimate of **x** is based on the cluster of images associated to the LOS link.

The procedure is shortly summarized in the following. To begin with, Let us consider the vectorized form of the channel $\mathbf{h} = \mathbf{\Psi}\mathbf{z}$, where $\mathbf{\Psi}$ is referred to as *dictionary* and **z** is the representation of **h** in $\mathbf{\Psi}$ [P6]. Now a single *atom* is a column vector of this dictionary (and corresponds to the vectorization of a multidimensional spatial-temporal discrete Fourier frequency).

Furthermore, we define a *dictionary function* $\mathcal{D}$ as

$$\mathbf{\Psi} = \mathcal{D}(\mathbf{\Xi})$$

which translates the dictionary variables to the atoms in dictionary.

Dictionary function is defined as a Kronecker product of U vectors and discrete complex-frequency components **v**

$$\mathcal{D}(\mathbf{\Xi}) \triangleq \left[\bigotimes_{i=1}^{U} \mathbf{v}(\xi_{i1}, K_i), \cdots, \bigotimes_{i=1}^{U} \mathbf{v}(\xi_{iL}, K_i)\right],$$

where the parameter *U* refers to the number of dimensions used to represent the spatial-temporal discrete frequencies and **v** is the discrete complex-frequency

$$\mathbf{v}(x, K) = \left[1, \cdots, e^{-j2\pi x(K-1)}\right]^{\mathrm{T}}.$$

For instance, if the MIMO-OFDM channel can be represented with a bi-dimensional spatial frequency and a mono-dimensional Fourier frequency, U equals to three. [P7]

Then a single location image, given the dictionary variable ξ_{il} from the channel estimation procedure, can be written

$$\tilde{\mathbf{x}}_l = \mathbf{b} + \begin{bmatrix} \frac{c\sqrt{1-u_{2l}^2}}{\Delta_f}\cos(\text{asin}(u_{1l})\,\text{sec}(\sin(u_{2l})))u_{3l} \\ -\frac{c\sqrt{1-u_{2l}^2}}{\Delta_f}\sin(\text{asin}(u_{1l})\,\text{sec}(\sin(u_{2l})))u_{3l} \\ -\frac{c\sqrt{1-u_{2l}^2}}{\Delta_f}u_{2l}u_{3l} \end{bmatrix}$$

where u_{il} is received from

$$u_{il} = \begin{cases} 2\xi_{il}, & 0 \le \xi_{il} < 0.5, \\ 2\xi_{il} - 2, & 0.5 \le \xi_{il} < 1. \end{cases}$$

As proposed in [P7], practical solution can be found via Adaptive-LASSO (A-LASSO) described in [P6], [P9]. Key points of the A-LASSO estimator is dictionary adaptation. First, the sparse coefficient, which can be seen as importance weights for the corresponding dictionary vectors, are used to resample the dictionary vectors. Then using new vectors replace each resampled vector with close parameters (grid). Dictionary vectors are updated until the required level of saturation is received. The example of the dictionary *atom* updates is illustrated in Figure 21. The example shows first the initial dictionary, where the elements are aligned on evenly spaced grid (upper left), then (upper right) each element on the grid is updated with its importance weight (black dots), and re-sampling method is used to calculate the new set of atoms (red dots). Finally the step 4 (lower right) shows the atoms concentrated on the 3 locations on a beamspace.

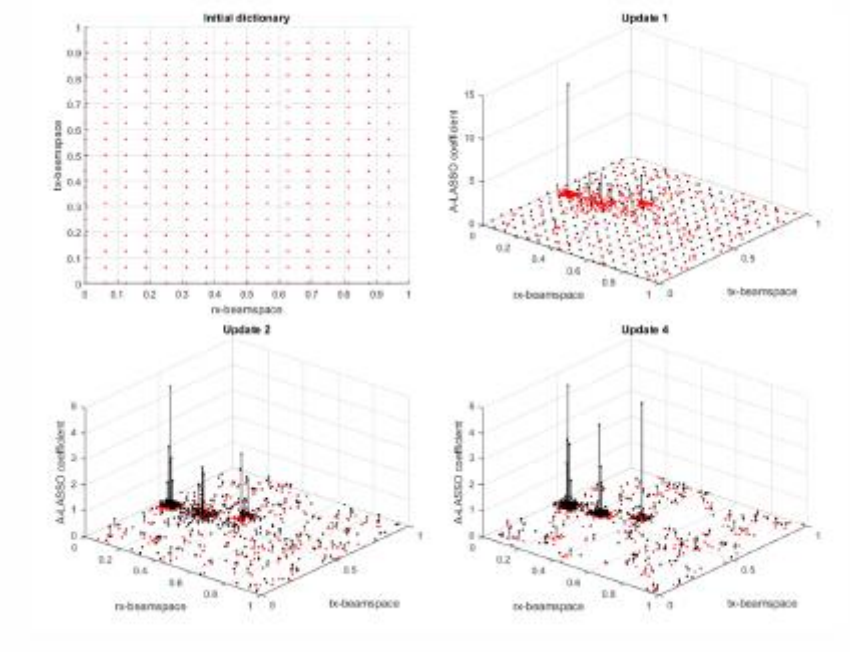

Figure 21: Four updates of dictionary column vectors inside the A-LASSO algorithm

Finally the set of location images a classified via K-nearest algorithm or as proposed in [P7] via Gaussian Mixture Model (GMM) to identify strongest beamspace component as a LOS path. And the location estimate is location image of the atom with the highest importance weight as

$$\hat{\mathbf{x}} = \hat{\boldsymbol{\mu}}_s, \quad \text{with } s = \arg\max \gamma_i,$$

where γ_i is the weight of cluster *i* in the location image domain, and $\hat{\boldsymbol{\mu}}_s$ is Gaussian Model parameter defining the cluster *s*. We utilize a classic Expectation-Maximization (EM) method to solve a classification problem. EM algorithm is well known, classical solution to the GMM problem. [P8]

3.4 Positioning Performance Analysis

In this Section, we give a performance analysis of the position and rotation estimation for the beamforming techniques described in previous Sections. Namely, we will investigate the impact of the different search strategies as well as the codebook size. Analysis is based on the publications [P12]. Analysis provided in this Section is with fixed subcarrier spacing, namely Δf = 75 kHz. The selected subcarrier spacing is matching the one used with the PoC system. Further analysis about the effect of the subcarrier spacing we refer to the publication [P11].

3.4.1 Performance metrics

We consider two performance metrics: effective data rate and position-rotation –error bound (PREB):

- **Effective data rate:**
  Assuming the beams selected for data transmission, after beam alignment, are **w** and **f**, then
  $$R = B\left(1 - \frac{T_t}{T_r}\right)\log_2\left(1 + \frac{|h|^2 P_{\text{tx}} S(\mathbf{w}, \mathbf{f}, \theta, \phi)}{\sigma^2}\right)$$
  where B is bandwidth, T_t and T_r are training time and frame time (as depicted in Figure 16) and
  $$S(\mathbf{w}, \mathbf{f}, \theta, \phi) \triangleq |\mathbf{w}^H \mathbf{a}_M(\theta)|^2 |\mathbf{f}^H \mathbf{a}_N(\phi)|^2$$
  is combined array and beamforming gain factor.

- **Position-Rotation error bound:**
  Assuming a total of K number of transmit/receive beam combinations to be used, we can compute the Fischer-Information –Matrix (FIM) to be associated with the position **p** and rotation **α**. The PREB is the inverse of thisFIM, and provides lower bounds, in the positive semi-definite sense on the achievable estimation accuracy. The mathematical definition of PREB is provided in [P10].

Generally, increasing the number of training beams will improve the PREB, but also lead to an increase in time allocated to training in frame. However, we shall see that based upon the searching strategy, the increase of training time does not always compromise the rate increase rate. In addition, that tension between rate and PREB does not always subsist. Our goal is to understand and quantify this trade-off.

3.4.2 Simulation results

We focus on an idealized MIMO-orthogonal frequency-division multiplexing (OFDM) communication system with 2048 subcarriers, time-frequency efficiency equal to one, inter-carrier spacing Δf = 75 kHz, fixed transmission power P_{tx} = 30 dBm, and carrier frequency 28 GHz. To easen the analysis, we assume that the number of antenna elements on BS and MS side same N = M.

Then one beam during beam alignment corresponds to one OFDM symbol, so T_{sym} = 13 μs and $E_s = P_{tx} T_{sym}$. Finally, we consider a radio frame with number of T_r / (η T_{sym}) OFDM symbols, where η is the OFDM time-efficiency, e.g, η = 0.93.

The MS location is at a fixed distance of 100 m to the BS (corresponding to SNR 0 ≈ 20 dB) and α = 0° (no rotation). We study two cases, namely φ = 0° and φ = 20°, that allows us to analyze the effect of beam misalignment.

First to illustrate the effect of different strategies in terms of the training overhead (number of slots), we show the overhead as number of training slots as a function of the number of antenna elements in Figure 22. More specifically, we show the overhead for exhaustive search and the hierarchical search two different settings, namely we consider a binary (K = 2) and ternary (K = 3) partitioning of search algorithm.

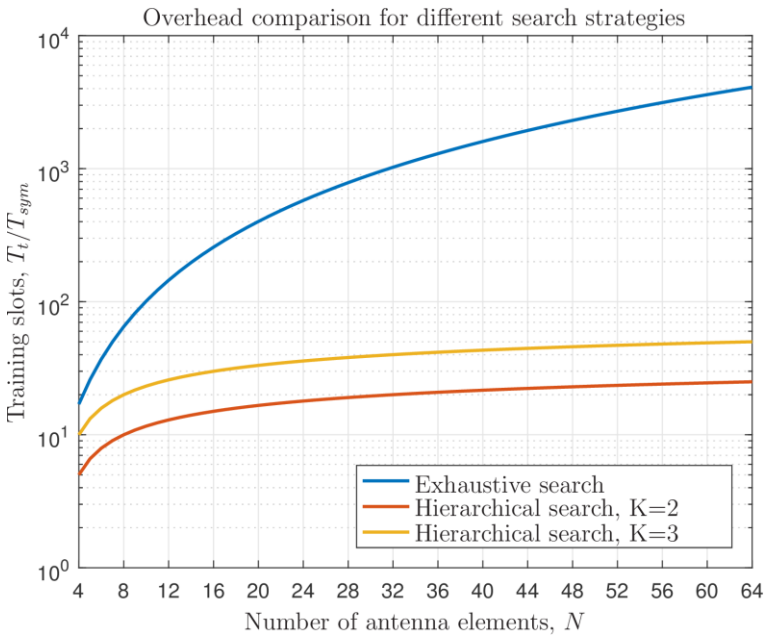

Figure 22: Comparison of different training strategies in terms of training slots.

Then we look into achievable data rate. The first result is illustrated in Figure 23 and it shows the achievable rate as a function of the frame length T_r with the exhaustive and hierarchical training strategies. Two values for antenna size N are considered, namely, N = 8 and N = 32. Let us focus first on the exhaustive search (blue lines) and compare the case between N = 8 (solid line) and N = 32 (dashed line). It can be noticed that for $T_r \leq 55$ ms the highest rate is

achieved with N = 8. This is due to high rate-loss caused by the training of N = 32 beams per transmit and receiver. In contrast, with the hierarchical search (red lines) the highest rate is achieved with N = 32 (dashed line) despite of the frame length.

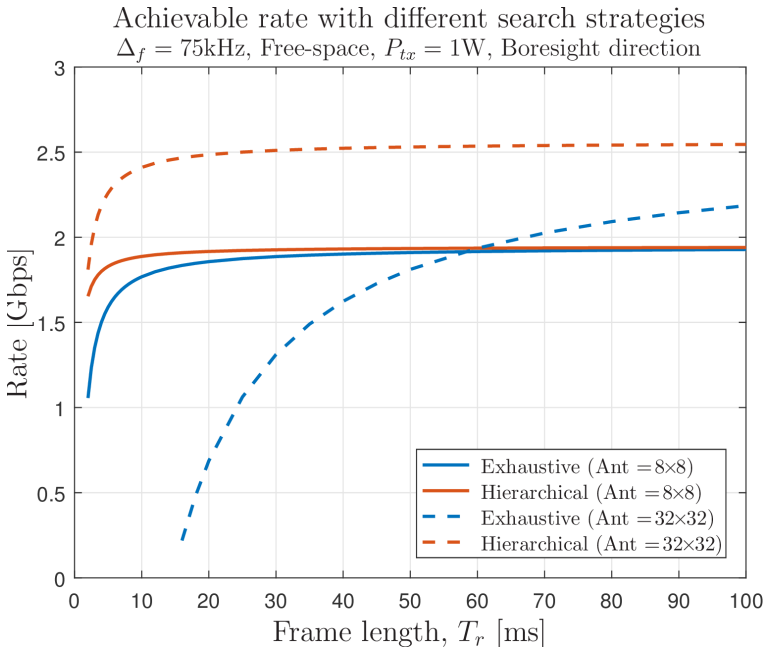

Figure 23: Comparison on the achievable rate with perfect beam-channel alignment. Rate as a function of the frame length and varying the number of antennas.

The next result, shown in Figure 24, tackles the problem of beam misalignment and, more specifically, we evaluate the effective rate as a function of the training time (obtained by varying the number of antennas) by changing the location of the receiver. Also in this plot, it can be noticed the exhaustive search strategy has an optimum training time whereas the rate achieved with hierarchical search grows despite the increase of T_t. More importantly, the rate obtained with the exhaustive search is also function of the φ and oscillates based upon the choice of T_t as, the latter depends on N, thus on the beamformers in the codebook. This phenomenon is not visible with the hierarchical search as the codebook is denser in the angular domain.

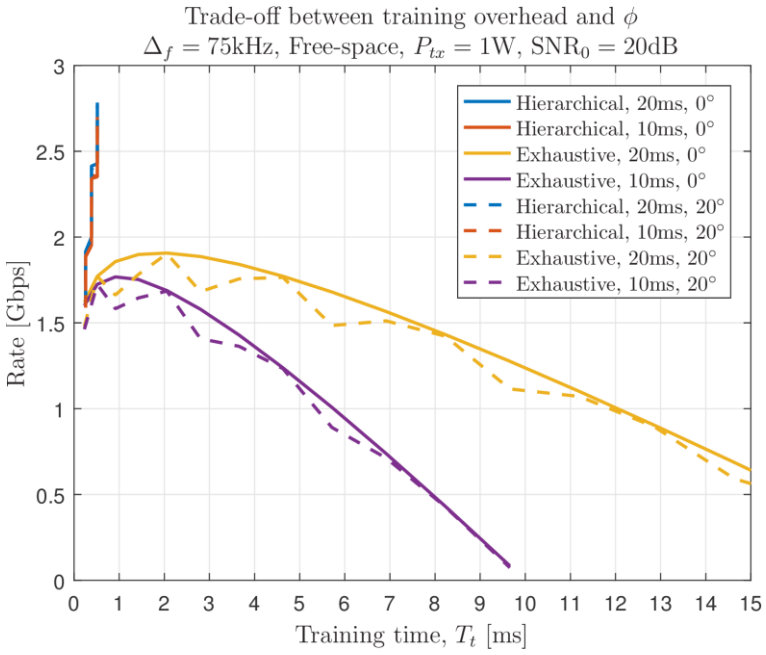

Figure 24: Comparison on the achievable rate with perfect beam-channel alignment. Rate as function of the training time and varying the location.

Next, we study the trade-off between positioning performance and effective data-rate. As mentioned in previous Section, positioning information can increase with the number of sounded beam pairs. If the training period is used also for positioning, then the longer the training, the lower the positioning error. Therefore, quantifying the achievable positioning error and assess which strategy can provide the best positioning performance are our first objectives.

Figure 25 shows the progress of the position error bound (PEB) as a function of the number of training slots. More specifically, the result refers to a set-up with N = M = 32 antennas, φ = 0º and φ = 20º. Our first observation is that better positioning performance can be achieved with the hierarchical search despite of the short number of training slots. In fact, by progressively aligning the beams more information is captured. Also, due to a sufficient density of beamformers, the performance is invariant with respect to φ. In contrast, the exhaustive search yields a larger location error that ultimately remains invariant with φ.

However, the progress of the PEB depends on the location and on the sweeping order of the beams. In the proposed simulation, the boresight direction is the first to be sounded by both transmitter and receiver. Therefore, with φ = 0º, the lowest PEB is reached already after the first sweep. Necessary condition for the inversion of the position FIM is that both transmitter and receiver sounds the channel with at least two beams [P10]. In addition, there is no increase of information (decrease of error), as all transmitter and receiver beams, but the boresight, have a null at φ = 0º. On the other hand, with φ = 20º, none of the codebook beamformers have neither maximum gain or null at φ. Thus, a continuous descend of the error occurs.

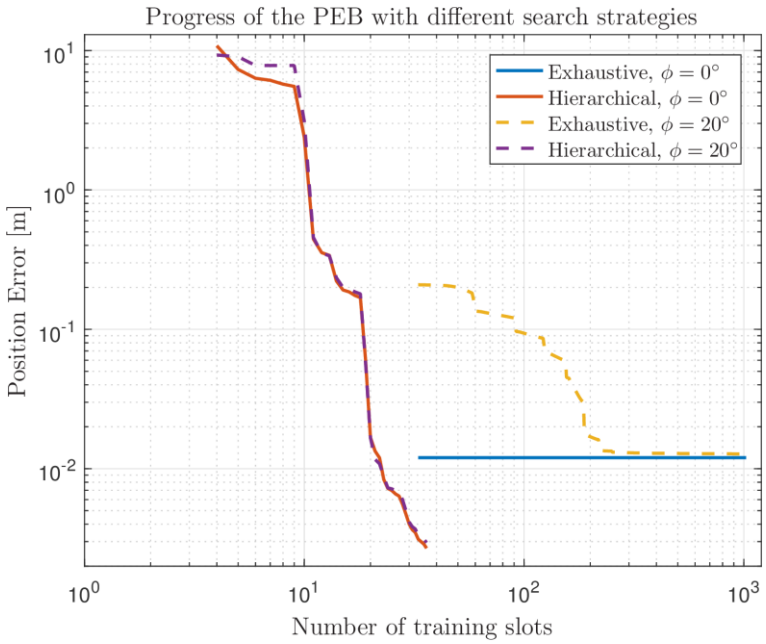

Figure 25: Position error bound as function of number of slots used in Exhaustive vs Hierarchical search strategies. SNR= 20dB in a Boresight (φ = 0 ◦) and misalignment (φ = 20 ◦) scenarios.

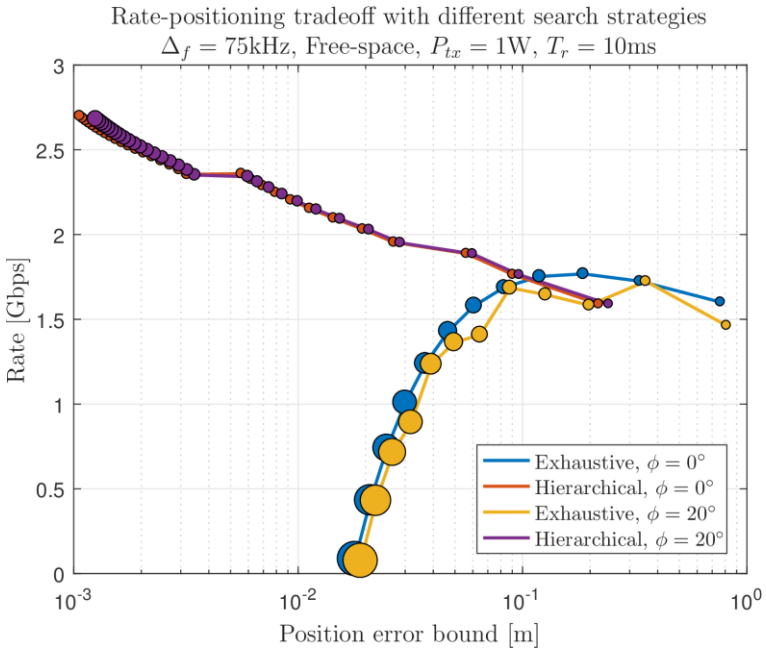

Figure 26: Comparison of the relationship between rate and PEB. A trade-off is noticeable with the exhaustive search. The size of the markers (circle size) are denoting the growing the number of antennas (thus also the growth of the codebook size).

Finally, Figure 26 shows the relationship between effective and rate and positioning error with different searching strategies. Also, the results are drawn with $\varphi = 0^o$, $\varphi = 20^o$ and the size of each marker is proportional to the overhead With an exhaustive search a trade-off must be met to either increase the rate or decrease the position error. The reason of this trade-off is the time-inefficiency of the training. In contrast, the relationship between PEB and rate with the hierarchical training does not show any trade-off. Indeed, increasing the rate will also increase the positioning performance. Furthermore, the dependency with φ is only noticeable with the exhaustive search.

4 Mixed GNSS/mmWave solution

4.1 Concept

This section describes the mixed positioning solution to be developed to cope with satellite availability and multipath in urban environment. It mainly relies on the pseudo-ranges provided by GNSS, with additional angular information provided by the 5G network that lowers the number of GNSS satellites required to compute a position and that can be used to dismiss GNSS signals affected by multipath (Figure 27) and to improve the location accuracy.

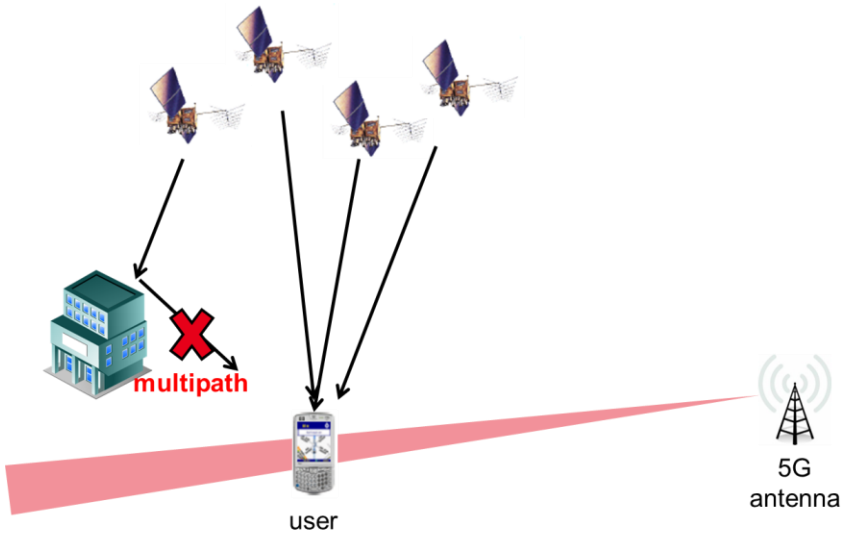

Figure 27: Mixed GNSS/mmWave solution

In order to understand the solution using both GNSS and 5G network, a short description is first made about the GNSS positioning solution. Then the information provided by the 5G network is analyzed and finally it is included in the GNSS solution. As the 5G line of sight (LoS) information provides extra equations to solve the positioning problem, one can remove GNSS equations (i.e. satellites).

4.2 Algorithm description

4.2.1 Position calculation

4.2.1.1 Traditional GNSS solution

This section summarizes the steps to solve the equations used in GNSS positioning. The initial equations are as follows:

$$\rho_i = \sqrt{(x_i - x_u)^2 + (y_i - y_u)^2 + (z_i - z_u)^2} + c \cdot t_u$$

Where ρ_i is the distance between the i[th] satellite and the user, (x_i, y_i, z_i) is the satellite position, (x_u, y_u, z_u) is the user's position and t_u is the user's clock bias. $\rho_i$is calculated by the receiver thanks to the time delay between emission and reception, (x_i, y_i, z_i) is provided

through the navigation message, so (x_u, y_u, z_u) and t_u are the 4 unknowns. Therefore, at least 4 equations (i.e. 4 satellites) are needed to compute a solution.

The method to solve the system of equations is iterative: the position is assumed and at the end of the iteration, the computed position is closer to the real one. The variables $\widehat{\ }$ are the assumed ones.

$$\rho_u = \widehat{\rho_u} + \Delta\rho_u$$
$$x_u = \widehat{x_u} + \Delta x_u$$
$$y_u = \widehat{y_u} + \Delta y_u$$
$$z_u = \widehat{z_u} + \Delta z_u$$
$$t_u = \widehat{t_u} + \Delta t_u$$

After this step, the unknowns are $(\Delta x_u, \Delta y_u, \Delta z_u)$ and Δt_u. The initial equation becomes:

$$f(x_u, y_u, z_u, t_u) = \rho_i = \sqrt{(x_i - \widehat{x_u} - \Delta x_u)^2 + (y_i - \widehat{y_u} - \Delta y_u)^2 + (z_i - \widehat{z_u} - \Delta z_u)^2} + c \cdot (\widehat{t_u} + \Delta t_u)$$

In order to solve a linear problem which is easier, Taylor series are used up to the first term.

$$f(x_u, y_u, z_u, t_u) \cong f(\widehat{x_u}, \widehat{y_u}, \widehat{z_u}, \widehat{t_u}) + \frac{\partial f(\widehat{x_u}, \widehat{y_u}, \widehat{z_u}, \widehat{t_u})}{\partial \widehat{x_u}} \Delta x_u + \frac{\partial f(\widehat{x_u}, \widehat{y_u}, \widehat{z_u}, \widehat{t_u})}{\partial \widehat{y_u}} \Delta y_u + \frac{\partial f(\widehat{x_u}, \widehat{y_u}, \widehat{z_u}, \widehat{t_u})}{\partial \widehat{z_u}} \Delta z_u + \frac{\partial f(\widehat{x_u}, \widehat{y_u}, \widehat{z_u}, \widehat{t_u})}{\partial \widehat{t_u}} \Delta t_u$$

$$\rho_i = \widehat{\rho_i} - \frac{(x_i - \widehat{x_u})}{\widehat{r_i}} \Delta x_u - \frac{(y_i - \widehat{y_u})}{\widehat{r_i}} \Delta y_u - \frac{(z_i - \widehat{z_u})}{\widehat{r_i}} \Delta z_u + c \cdot t_u$$

Where

$$\widehat{\rho_i} = \sqrt{(x_i - \widehat{x_u})^2 + (y_i - \widehat{y_u})^2 + (z_i - \widehat{z_u})^2} + c \cdot \widehat{t_u}$$
$$\widehat{r_i} = \sqrt{(x_i - \widehat{x_u})^2 + (y_i - \widehat{y_u})^2 + (z_i - \widehat{z_u})^2}$$

Intuitive explanation (no clock bias)

If one assumes that there is no clock bias and makes the substitution where (x_u, y_u, z_u) and t_u are the unknowns, the equation of a satellite represents the plane:

- tangent to the circle with the satellite at its center and of radius ρ_i

- and perpendicular to the line of sight between the satellite and the assumed position.

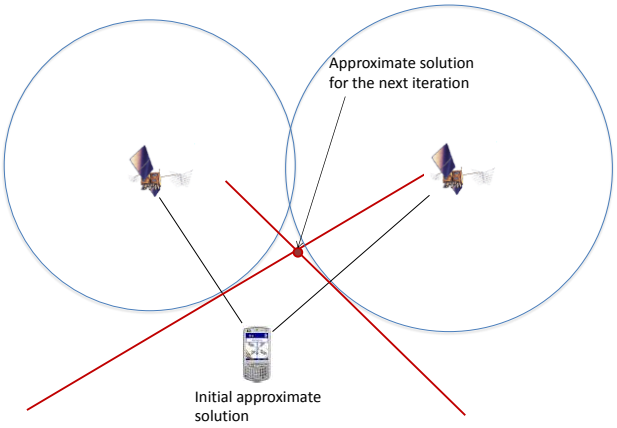

Figure 28: Illustration of GNSS equations

5G information to fit GNSS equations

5G antennas shall provide the direction towards the receiver that needs to be located. It is assumed that the azimuth and elevation angles are provided in real time and that the position of the 5G station is well known. With that information, one has to define one planes that will fit in the GNSS solution. The planes are described as follows:

- Azimuth plane is a vertical plane in the local reference that contains the location of both the station and the receiver.
- Elevation plane is a plane perpendicular to the azimuth plane that contains the location of both the station and the receiver

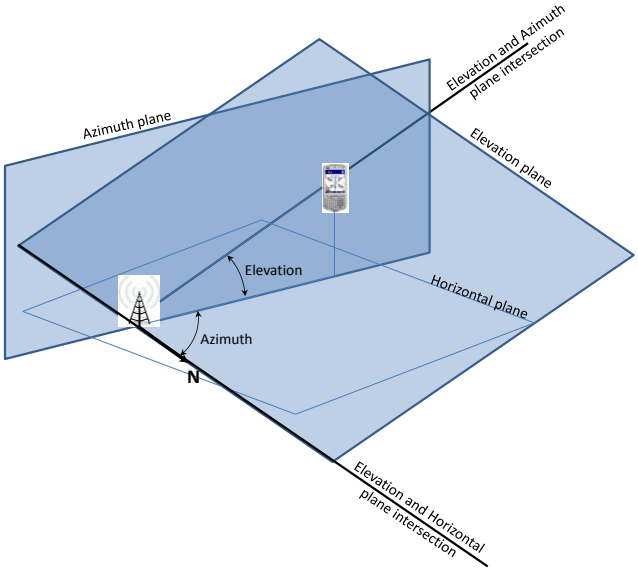

Figure 29: Illustration of 5G equations

The planes can be calculated as follows in the ECEF frame:

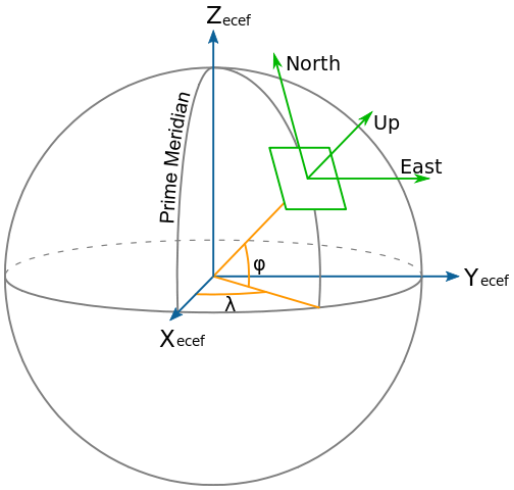

Figure 30: ECEF frame

Let $\vec{u} = (X_u, Y_u, Z_u)$ be the vertical vector at the station location. To complete the reference frame, the vector in the east direction will be:

$$\vec{e} = -\frac{(\vec{u} \times \vec{Z})}{|\vec{u} \times \vec{Z}|} = -\frac{\begin{vmatrix} \vec{\imath} & \vec{\jmath} & \vec{k} \\ X_u & Y_u & Z_u \\ 0 & 0 & 1 \end{vmatrix}}{|\vec{u} \times \vec{Z}|} = \left(\frac{-Y_u}{\sqrt{{X_u}^2 + {Y_u}^2}}, \frac{X_u}{\sqrt{{X_u}^2 + {Y_u}^2}}, 0 \right)$$

Where $\vec{Z}$ is the vector in the Z direction in the ECEF reference. Then, the north vector completes the reference:

$$\vec{n} = \frac{(\vec{u} \times \vec{e})}{|\vec{u} \times \vec{e}|}$$

Once the local reference is set, it is easy to find the extra planes provided by the 5G antenna. Naming of the variables:

- az is the azimuth angle
- $\overrightarrow{az}$ is the unitary vector in the direction of the receiver in the local horizontal plane
- $\overrightarrow{azp}$ is the normal vector of the azimuth plane

Analogous definitions apply for the elevation.

The strategy is to find the vector perpendicular to the plane and a point in the plane (station position) to build the plane equation. To do so, the vector included in the plane needs to be calculated:

$$\overrightarrow{az} = \cos(az) \cdot \vec{n} + \sin(az) \cdot \vec{e}$$

Together with another vector in the plane (the vertical vector):

$$\overrightarrow{azp} = \overrightarrow{az} \times \vec{u}$$

The azimuth plane equation is therefore:

$$\overrightarrow{azp} \cdot \begin{pmatrix} x_u - X_S \\ y_u - Y_S \\ z_u - Z_S \end{pmatrix} = 0$$

Where $\overrightarrow{P_S} = (X_S, Y_S, Z_S)$ is the station position.

The same strategy applies for the elevation angle:

$$\overrightarrow{el} = \cos(el) \cdot \overrightarrow{az} + \sin(el) \cdot \frac{\vec{u}}{|u|}$$

$$\overrightarrow{elp} = \overrightarrow{el} \times \overrightarrow{azp}$$

$$\overrightarrow{elp} \cdot \begin{pmatrix} x_u - X_S \\ y_u - Y_S \\ z_u - Z_S \end{pmatrix} = 0$$

4.2.1.2 Mixed solution

If the linearized equation for the satellites is changed so that the variable is the user position and not anymore the delta between the assumed position and the true one, one gets the following expression:

$$\rho_i = \widehat{\rho_i} - \frac{(x_i - \widehat{x_u})}{\widehat{r_i}}(x_u - \widehat{x_u}) - \frac{(y_i - \widehat{y_u})}{\widehat{r_i}}(y_u - \widehat{y_u}) - \frac{(z_i - \widehat{z_u})}{\widehat{r_i}}(z_u - \hat{z}) + c \cdot t_u$$

It can be reformulated as:

$$\frac{(x_i - \widehat{x_u})}{\widehat{r_i}}x_u + \frac{(y_i - \widehat{y_u})}{\widehat{r_i}}y_u + \frac{(z_i - \widehat{z_u})}{\widehat{r_i}}z_u + c \cdot t_u = \widehat{\rho_i} - \rho_i + \frac{(x_i - \widehat{x_u})\widehat{x_u}}{\widehat{r_i}} + \frac{(y_i - \widehat{y_u})\widehat{y_u}}{\widehat{r_i}} + \frac{(z_i - \widehat{z_u})\widehat{z_u}}{\widehat{r_i}}$$

The 5G equations can be expressed in this way

$$azp_x x_u + azp_y y_u + azp_z z_u + 0 \cdot t_u = azp_x X_s + azp_y Y_s + azp_z Z_s$$

Finally, with 2 satellite equations, the system to solve would be:

$$\begin{pmatrix} \frac{(x_i - \widehat{x_u})}{\widehat{r_i}} & \frac{(y_i - \widehat{y_u})}{\widehat{r_i}} & \frac{(z_i - \widehat{z_u})}{\widehat{r_i}} & c \\ \frac{(x_j - \widehat{x_u})}{\widehat{r_j}} & \frac{(y_j - \widehat{y_u})}{\widehat{r_j}} & \frac{(z_j - \widehat{z_u})}{\widehat{r_j}} & c \\ azp_x & azp_y & azp_z & 0 \\ elp_x & elp_y & elp_z & 0 \end{pmatrix} \cdot \begin{pmatrix} x_u \\ y_u \\ z_u \\ t_u \end{pmatrix}$$

$$= \begin{pmatrix} \widehat{\rho_i} - \rho_i + \frac{(x_i - \widehat{x_u})\widehat{x_u}}{\widehat{r_i}} + \frac{(y_i - \widehat{y_u})\widehat{y_u}}{\widehat{r_i}} + \frac{(z_i - \widehat{z_u})\widehat{z_u}}{\widehat{r_i}} \\ \widehat{\rho_j} - \rho_j + \frac{(x_j - \widehat{x_u})\widehat{x_u}}{\widehat{r_j}} + \frac{(y_j - \widehat{y_u})\widehat{y_u}}{\widehat{r_j}} + \frac{(z_j - \widehat{z_u})\widehat{z_u}}{\widehat{r_j}} \\ azp_x X_s + azp_y Y_s + azp_z Z_s \\ elp_x X_s + elp_y Y_s + elp_z Z_s \end{pmatrix}$$

4.2.1 Residual calculation

The residual calculation for this algorithm will be used to sort out the solutions that may contain a multipath. The hypothesis of the algorithm is that the 5G technology is not affected by multipath. The residual calculated here is the distance between the computed calculation and the plane provided by the 5G algorithm.

If the equation of a plane is:

$$ax + by + cz + d = 0$$

Then: (a, b, c) is the vector normal to the plane. We consider that its modulus is 1.

The point to be considered is: (x_u, y_u, z_u)

Then $(x, y, z) = (x_u, y_u, z_u) + \lambda(a, b, c)$ is the equation of the line that passes through the point and that is perpendicular to the plane. Together with the position of the plane:

$$a(x_u + \lambda a) + b(y_u + \lambda b) + c(z_u + \lambda c) + d = 0$$

Then the residual λ is the distance between the point and the plane:

$$\lambda = abs\left(\frac{d + ax_u + by_u + cz_u}{a^2 + b^2 + c^2}\right)$$

4.2.2 KPI calculation

The KPI (key performance indicator) that will be used is the DOP (dilution of precision) of the computed solution. This term is generally used in the GNSS to account both for the accuracy of the satellite to receiver distance computation and the geometry of the satellites.

The equation used to compute the position is:

$$\begin{pmatrix} \frac{(x_i - \widehat{x_u})}{\widehat{r_i}} & \frac{(y_i - \widehat{y_u})}{\widehat{r_i}} & \frac{(z_i - \widehat{z_u})}{\widehat{r_i}} & c \\ \frac{(x_j - \widehat{x_u})}{\widehat{r_j}} & \frac{(y_j - \widehat{y_u})}{\widehat{r_j}} & \frac{(z_j - \widehat{z_u})}{\widehat{r_j}} & c \\ azp_x & azp_y & azp_z & 0 \\ elp_x & elp_y & elp_z & 0 \end{pmatrix} \cdot \begin{pmatrix} x_u \\ y_u \\ z_u \\ t_u \end{pmatrix}$$

$$= \begin{pmatrix} \widehat{\rho_i} - \rho_i + \frac{(x_i - \widehat{x_u})\widehat{x_u}}{\widehat{r_i}} + \frac{(y_i - \widehat{y_u})\widehat{y_u}}{\widehat{r_i}} + \frac{(z_i - \widehat{z_u})\widehat{z_u}}{\widehat{r_i}} \\ \widehat{\rho_j} - \rho_j + \frac{(x_j - \widehat{x_u})\widehat{x_u}}{\widehat{r_j}} + \frac{(y_j - \widehat{y_u})\widehat{y_u}}{\widehat{r_j}} + \frac{(z_j - \widehat{z_u})\widehat{z_u}}{\widehat{r_j}} \\ azp_x X_s + azp_y Y_s + azp_z Z_s \\ elp_x X_s + elp_y Y_s + elp_z Z_s \end{pmatrix}$$

Making a change of variables…

$$x_u = \widehat{x_u} + \Delta x_u$$
$$y_u = \widehat{y_u} + \Delta y_u$$
$$z_u = \widehat{z_u} + \Delta z_u$$
$$t_u = \widehat{t_u} + \Delta t_u$$

…the equation can be written as:

$$\begin{pmatrix} \frac{(x_i-\widehat{x_u})}{\widehat{r_i}} & \frac{(y_i-\widehat{y_u})}{\widehat{r_i}} & \frac{(z_i-\widehat{z_u})}{\widehat{r_i}} & c \\ \frac{(x_j-\widehat{x_u})}{\widehat{r_j}} & \frac{(y_j-\widehat{y_u})}{\widehat{r_j}} & \frac{(z_j-\widehat{z_u})}{\widehat{r_j}} & c \\ azp_x & azp_y & azp_z & 0 \\ elp_x & elp_y & elp_z & 0 \end{pmatrix} \cdot \begin{pmatrix} \Delta x_u \\ \Delta y_u \\ \Delta z_u \\ \Delta t_u \end{pmatrix}$$

$$= \begin{pmatrix} \widehat{\rho_i} - \rho_i \\ \widehat{\rho_j} - \rho_j \\ azp_x X_s + azp_y Y_s + azp_z Z_s - azp_x\widehat{x_u} - azp_y\widehat{y_u} - azp_z\widehat{z_u} \\ elp_x X_s + elp_y Y_s + elp_z Z_s - elp_x\widehat{x_u} - elp_y\widehat{y_u} - elp_z\widehat{z_u} \end{pmatrix}$$

Or in a matrix form:$\mathrm{H} \cdot \Delta x = \Delta\rho$

Note that $\Delta\rho$ is a notation taken from the GNSS domain, but for the 5G equations, it represents the distance between the position and the plane.

Then the new position vector is:

$$\Delta x = \mathrm{H}^{-1} \cdot \Delta\rho$$

The associated covariance matrix is:

$$(\sigma\mathrm{H}^T \cdot \sigma\mathrm{H})^{-1}$$

Usually, the variance σ^2 is the ${\sigma_{UERE}}^2$ but in this case, one has to account for the 5G equations which will not have the same variance. ${\sigma_{UERE}}^2$ is the variance of the User Equivalent Range Error, or in other words the variance of the error made in the calculation of the pseudo-range. For the 5G positioning equations, it will be necessary to change that error variance.

Therefore,

$$H \cdot \sigma = \begin{pmatrix} \frac{(x_i-\widehat{x_u})}{\widehat{r_i}}\sigma_{UERE} & \frac{(y_i-\widehat{y_u})}{\widehat{r_i}}\sigma_{UERE} & \frac{(z_i-\widehat{z_u})}{\widehat{r_i}}\sigma_{UERE} & c\cdot\sigma_{UERE} \\ \frac{(x_j-\widehat{x_u})}{\widehat{r_j}}\sigma_{UERE} & \frac{(y_j-\widehat{y_u})}{\widehat{r_j}}\sigma_{UERE} & \frac{(z_j-\widehat{z_u})}{\widehat{r_j}}\sigma_{UERE} & c\cdot\sigma_{UERE} \\ azp_x\cdot\sigma_{5G} & azp_y\cdot\sigma_{5G} & azp_z\cdot\sigma_{5G} & 0 \\ elp_x\cdot\sigma_{5G} & elp_y\cdot\sigma_{5G} & elp_z\cdot\sigma_{5G} & 0 \end{pmatrix}$$

4.2.3 Computation of observations variance

Observation vector is given by the following formula:

$$\begin{pmatrix} \widehat{\rho_i} - \rho_i \\ \widehat{\rho_j} - \rho_j \\ azp^T \cdot R \\ elp^T \cdot R \end{pmatrix}$$

With $R = \begin{pmatrix} X_S - \widehat{x_u} \\ Y_S - \widehat{y_u} \\ Z_S - \widehat{z_u} \end{pmatrix} \in \mathbb{R}^{3\times 1}$ is the distance between the 5G station and the estimated user position which is assumed to be known at this stage of the derivation.

The covariance matrix of observations is as follow:

$$\Sigma = \begin{pmatrix} var(\widehat{\rho_i} - \rho_i) & cov(\widehat{\rho_i} - \rho_i, \widehat{\rho_j} - \rho_j) & cov(\widehat{\rho_i} - \rho_i, azp^T \cdot R) & cov(\widehat{\rho_i} - \rho_i, elp^T \cdot R) \\ cov(\widehat{\rho_j} - \rho_j, \widehat{\rho_i} - \rho_i) & var(\widehat{\rho_j} - \rho_j) & cov(\widehat{\rho_j} - \rho_j, azp^T \cdot R) & cov(\widehat{\rho_j} - \rho_j, elp^T \cdot R) \\ cov(azp^T \cdot R, \widehat{\rho_i} - \rho_i) & cov(azp^T \cdot R, \widehat{\rho_j} - \rho_j) & var(azp^T \cdot R) & cov(azp^T \cdot R, elp^T \cdot R) \\ cov(elp^T \cdot R, \widehat{\rho_i} - \rho_i) & cov(elp^T \cdot R, \widehat{\rho_j} - \rho_j) & cov(elp^T \cdot R, azp^T \cdot R) & var(elp^T \cdot R) \end{pmatrix}$$

Moreover it is supposed that $\rho_i, \rho_j, azp^T \cdot R \; and \; elp^T \cdot R$ are independent variables and $\widehat{\rho_i} \; and \; \widehat{\rho_j}$ are scalar. The covariance matrix can be simplified as:

$$\Sigma = \begin{pmatrix} var(\rho_i) & 0 & 0 & 0 \\ 0 & var(\rho_j) & 0 & 0 \\ 0 & 0 & var(azp^T \cdot R) & cov(azp^T \cdot R, elp^T \cdot R) \\ 0 & 0 & cov(elp^T \cdot R, azp^T \cdot R) & var(elp^T \cdot R) \end{pmatrix}$$

4.2.3.1 GNSS measurements variance

As previously stated the variance of GNSS measurements are the User Equivalent Range Error (UERE). $var(\rho_i) = {\sigma_{UERE,i}}^2 \;\; \& \;\; var(\rho_j) = {\sigma_{UERE,j}}^2$

This variance is dependent on atmospheric (tropospheric and ionospheric), clock (transmitter and receiver), multipath, and ephemeris corrections.

4.2.3.2 5G measurements variance

Let us rewrite $\boldsymbol{azp} \; and \; \boldsymbol{elp}$ assuming east, north, up $(\boldsymbol{e}, \boldsymbol{n}, \boldsymbol{u})$ and $(\boldsymbol{az}, \boldsymbol{el})$ vectors are unitary vectors.

$$\begin{aligned} \boldsymbol{azp} = \; \boldsymbol{az} \times \boldsymbol{u} &= (\cos(az) \cdot \boldsymbol{n} + \sin(az) \cdot \boldsymbol{e}) \times \boldsymbol{u} = \cos(az) \cdot \boldsymbol{e} - \sin(az) \cdot \boldsymbol{n} \\ &= \boldsymbol{ENU} \cdot \begin{pmatrix} \cos(az) \\ -\sin(az) \\ 0 \end{pmatrix} \\ \boldsymbol{elp} = \boldsymbol{el} \times \boldsymbol{azp} &= (\cos(el) \cdot \boldsymbol{az} + \sin(el) \cdot \boldsymbol{u}) \times (\cos(az) \cdot \boldsymbol{e} - \sin(az) \cdot \boldsymbol{n}) \\ &= \sin(el)\sin(az) \cdot \boldsymbol{e} \\ &\quad + \sin(el)\cos(az) \cdot \boldsymbol{n} - \cos(\mathrm{el}). \boldsymbol{u} = \boldsymbol{ENU} \cdot \begin{pmatrix} \sin(el)\sin(az) \\ \sin(el)\cos(az) \\ -\cos(el) \end{pmatrix} \end{aligned}$$

$$\boldsymbol{ENU} = (\boldsymbol{e} \quad \boldsymbol{n} \quad \boldsymbol{u}) \in \mathbb{R}^{3\times 3}$$

Then:

$$COV[\boldsymbol{elp}^T \cdot \boldsymbol{R}, \boldsymbol{azp}^T \cdot \boldsymbol{R}] = \mathbb{E}[\boldsymbol{R}^T \cdot \boldsymbol{elp} \cdot \boldsymbol{azp}^T \cdot \boldsymbol{R}] - \mathbb{E}[\boldsymbol{elp}^T \cdot \boldsymbol{R}] * \mathbb{E}[\boldsymbol{azp}^T \cdot \boldsymbol{R}]$$
$$= \boldsymbol{R}^T \cdot \boldsymbol{ENU} \cdot \mathbb{E}\begin{bmatrix} \boldsymbol{sin(el)sin(az)cos(az)} & \boldsymbol{-sin(el)sin(az)^2} & \boldsymbol{0} \\ \boldsymbol{sin(el)cos(az)^2} & \boldsymbol{-sin(el)sin(az)cos(az)} & \boldsymbol{0} \\ \boldsymbol{-cos(el)cos(az)} & \boldsymbol{cos(el)cos(az)} & \boldsymbol{0} \end{bmatrix} \cdot \boldsymbol{ENU^T} \cdot \boldsymbol{R} - \boldsymbol{R}^T \cdot \boldsymbol{ENU}$$
$$\cdot \mathbb{E}\begin{bmatrix} \sin(el)\sin(az) \\ \sin(el)\cos(az) \\ -\cos(el) \end{bmatrix} \cdot \mathbb{E}[\cos(az) \quad -\sin(az) \quad \boldsymbol{0}] \cdot \boldsymbol{ENU^T} \cdot \boldsymbol{R} = \boldsymbol{R}^T \cdot \boldsymbol{ENU} \cdot \boldsymbol{\Sigma_{azp,el}} \cdot \boldsymbol{ENU^T} \cdot \boldsymbol{R}$$

$$\boldsymbol{\Sigma_{azp,el}} = \begin{pmatrix} cov[\boldsymbol{sin(el)sin(az)}, \boldsymbol{cos(az)}] & cov[\boldsymbol{sin(el)sin(az)}, \boldsymbol{-sin(az)}] & \boldsymbol{0} \\ cov[\boldsymbol{sin(el)cos(az)}, \boldsymbol{cos(az)}] & cov[\boldsymbol{sin(el)cos(az)}, \boldsymbol{-sin(az)}] & \boldsymbol{0} \\ cov[\boldsymbol{-cos(el)}, \boldsymbol{cos(az)}] & cov[\boldsymbol{-cos(el)}, \boldsymbol{-sin(az)}] & \boldsymbol{0} \end{pmatrix}$$

$$VAR[\boldsymbol{azp}^T \cdot \boldsymbol{R}] = \boldsymbol{R}^T \cdot \boldsymbol{ENU} \cdot \boldsymbol{\Sigma_{azp}} \cdot \boldsymbol{ENU}^T \cdot \boldsymbol{R}$$
$$\boldsymbol{\Sigma_{azp}} = \begin{pmatrix} var[\cos(az)] & cov[\cos(az), -\sin(az)] & \boldsymbol{0} \\ cov[\cos(az), -\sin(az)] & var[\sin(az)] & \boldsymbol{0} \\ \boldsymbol{0} & \boldsymbol{0} & \boldsymbol{0} \end{pmatrix}$$
$$VAR[\boldsymbol{elp}^T \cdot \boldsymbol{R}] = \boldsymbol{R}^T \cdot \boldsymbol{ENU} \cdot \boldsymbol{\Sigma_{elp}} \cdot \boldsymbol{ENU}^T \cdot \boldsymbol{R}$$
$$\boldsymbol{\Sigma_{elp}}$$
$$= \begin{pmatrix} var[\sin(el) * \sin(az)] & cov[\sin(el) * \sin(az), \sin(el) * \cos(az),] & cov[\sin(el) * \sin(az), -\cos(el)] \\ cov[\sin(el) * \cos(az), \sin(el) * \sin(az)] & var[\sin(el) * \cos(az)] & cov[\sin(el) * \cos(az), -\cos(el)] \\ cov[-\cos(el), \sin(el) * \sin(az)] & cov[-\cos(el), \sin(el) * \cos(az)] & var[\cos(el)] \end{pmatrix}$$

Using

$$\begin{cases} var[\sin(el) * \sin(az)] = \mathbb{E}[\sin(az)^2] * \mathbb{E}[\sin(el)^2] - \mathbb{E}[\sin(az)]^2 * \mathbb{E}[\sin(el)]^2 \\ var[\sin(el) * \cos(az)] = \mathbb{E}[\cos(az)^2] * \mathbb{E}[\sin(el)^2] - \mathbb{E}[\cos(az)]^2 * \mathbb{E}[\sin(el)]^2 \\ Cov[\sin(el)\cos(az), \sin(el)\sin(az)] = \mathbb{E}[\sin(el)^2] * \mathbb{E}[\sin(az)\cos(az)] - \mathbb{E}[\sin(el)]^2 * \mathbb{E}[\cos(az)] * \mathbb{E}[\sin(az)] \\ Cov[-\cos(el), \sin(el)\sin(az)] = \mathbb{E}[\sin(el)\cos(el)] * \mathbb{E}[\sin(az)] * (\mathbb{E}[\cos(el)] - 1) \\ Cov[-\cos(el), \sin(el)\cos(az)] = \mathbb{E}[\sin(el)\cos(el)] * \mathbb{E}[\cos(az)] * (\mathbb{E}[\cos(el)] - 1) \end{cases}$$

One can assume elevation and azimuth angles are independent random variables distributed normally with mean θ and variance σ².

$$az \sim N(\theta_{az}, \sigma_{az}^2) \quad \& \quad el \sim N(\theta_{el}, \sigma_{el}^2)$$

If α is a random variable $\alpha \sim N(\alpha_0, \sigma^2)$ distributed normally with mean α_0 and variance σ², then:

$$\mathbb{E}[\cos(\alpha)] = e^{-\frac{\sigma^2}{2}} * \cos(\alpha_0)$$
$$\mathbb{E}[\sin(\alpha)] = e^{-\frac{\sigma^2}{2}} * \sin(\alpha_0)$$
$$\mathbb{E}[\cos(\alpha)\sin(\alpha)] = \frac{1}{2} * e^{-2\sigma^2} * \sin(2\alpha_0)$$
$$\mathbb{E}[\cos(\alpha)^2] = \frac{1}{2} + \frac{1}{2} * e^{-2\sigma^2} * \cos(2\alpha_0)$$
$$\mathbb{E}[\sin(\alpha)^2] = \frac{1}{2} - \frac{1}{2} * e^{-2\sigma^2} * \cos(2\alpha_0)$$
$$VAR[\cos(\alpha)] = \frac{1}{2} + \frac{1}{2} * e^{-2\sigma^2} * \cos(2\alpha_0) - e^{-\sigma^2} * \cos(\alpha_0)^2$$
$$VAR[\sin(\alpha)] = \frac{1}{2} - \frac{1}{2} * e^{-2\sigma^2} * \cos(2\alpha_0) - e^{-\sigma^2} * \sin(\alpha_0)^2$$
$$COV[\cos(\alpha), \sin(\alpha)] = \frac{\sin(2\alpha_0)}{2} * [e^{-2\sigma^2} - e^{-\sigma^2}]$$

Since azimuth and elevation variances are expected to have small deviation (under 5deg), 1st order approximation can be done for simplified equations.

4.2.3.3 Sum Up

Variance of GNSS observations varies from variance of 5G observations due to the nature of the observations (range versus angle).

Variance of GNSS observations (UERE) may vary depending on the applied corrections.

Variance of 5G observations are depending on the geometry of the LOS. The variance is quadratic with the distance of the estimated position from the station. For calculation of the variance and covariance, the mean of random variable equals the observation value ($\alpha_0 = \theta_{az} = az_{observed}$).

4.3 Preliminary results and model validation

4.3.1 Purpose of simulations

Previous detailed equations describe functioning of the mixed GNSS-5G solution but do not provide the performance of such algorithm. The purpose of preliminary simulations is to anticipate tests in real conditions and assess the performance of the proposed algorithms in various environments. By running simulations one will avoid non desired test cases and bad combination of test inputs. For example, due to the variance of 5G measurements it can be inferred that mixed solution far from 5G stations will have bad results and conclude to a threshold distance for real test simulations. Running simulation can also assess the most suitable environment for the mixed solution that gives the best results (potentially better than the classic GNSS solution).

The following simulations are" run with real GNSS observations (rinex file) and simulated 5G observations.

4.3.2 Environmental conditions

User surroundings is split into 3 use cases which are urban, semi-urban and rural environment. Each environment differs from the other by the elevation mask angle and the proximity of the 5G station.

Urban environment:

- GNSS elevation mask=60deg
- range from 5G station to user=20m

Semi urban environment:

- GNSS elevation mask=30deg
- range from 5G station to user=50m

Rural environment:

- GNSS elevation mask=10deg
- range from 5G station to user=500m

For every cases, the 5G station position is chosen to be:

- 10m above the receiver height,
- At an azimuth angle of -45 deg from the user position.

Moreover, the accuracy of 5G station data is assumed to be 5 deg, which means 99 percent of the elevation and azimuth angles are under 5 deg of error.

4.3.3 Key Performance Indicator

The following key performance indicator (KPI) are used for assessment of the hybridization solution.

Availability: Percentage of time the position is available (calculable).

Horizontal and Vertical Accuracy: 99th percentile of true error on horizontal plane and vertical direction.

Norm of the residuals: 99th percentile of the norm of the residuals.

Dilution Of Precision (DOP): Geometry DOP, Horizontal DOP, Vertical DOP, Time DOP. The 99th percentile is provided.

4.3.4 Positioning solution

For each surrounding previously described several positioning solutions will be tested among:

- Classic GNSS solution: Broadcast ephemeris are used,
- Hybridization of GNSS and 5G solution with broadcast ephemeris,
- 5G Only solution. For this positioning solution one additional 5G station is added and only two stations are used for position calculation. The second station is at the same distance from the user and at 20 deg of azimuth.

4.3.5 Signal and constellation

Single frequency on L1 band is used.

Simulation is run under GPS constellation.

4.3.6 Preliminary results for GPS only

KPI	Environment	Classic GNSS	Classic GNSS & 5G	5G only (addition of 2nd station)
Availability [%]	Urban	2.1	55.8	100
	Semi Urban	91.1	100	100
	Rural	100	100	100
Horizontal accuracy (99th percentile)	Urban	9.46	164.54	1.47
	Semi Urban	13.47	8.42	4.14
	Rural	6.48	8.42	40.70

Vertical accuracy (99th percentile)	Urban	49.98	92.63	1.10
	Semi Urban	24.61	3.73	2.25
	Rural	18.19	17.41	20.85
Norm of the residuals [m]	Urban	113.42	97.48	1.14
	Semi Urban	48.94	40.65	3.34
	Rural	26.66	46.51	30.45
GDOP (99th percentile)	Urban	54.9	610.3	0.67
	Semi Urban	24.3	18.7	1.8
	Rural	4.88	9.4	17.9
PDOP (99th percentile)	Urban	39.9	544.1	0.67
	Semi Urban	19.9	17.9	1.8
	Rural	4.0	7.8	17.9
HDOP (99th percentile)	Urban	28.3	341.3	0.40
	Semi Urb.	15.2	12.9	1.2
	Rural	3.1	6.4	13.8
VDOP (99th percentile)	Urban	28.2	423.7	0.54
	Semi Urb.	16.1	12.0	1.2
	Rural	3.3	6.1	11.4
TDOP (99th percentile)	Urban	37.7	271.5	NA
	Semi Urb.	14.7	5.3	NA
	Rural	2.8	5.1	NA

4.3.6.1 Mixed solution in semi-urban environment

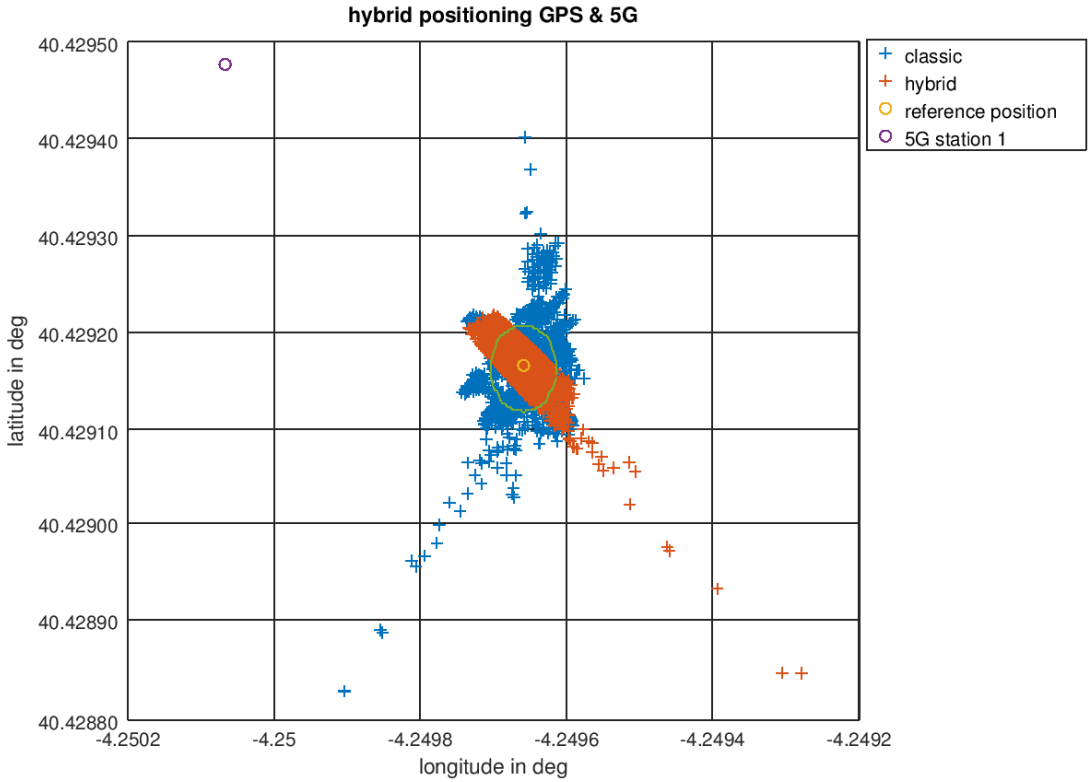

In semi urban environment the use of hybridized algorithm forces the solution to be close to the 5G line of sight (5deg accuracy, the green circle is 5m radius) and in this case to provide better accuracy.

4.3.6.2 Mixed solution in urban environment

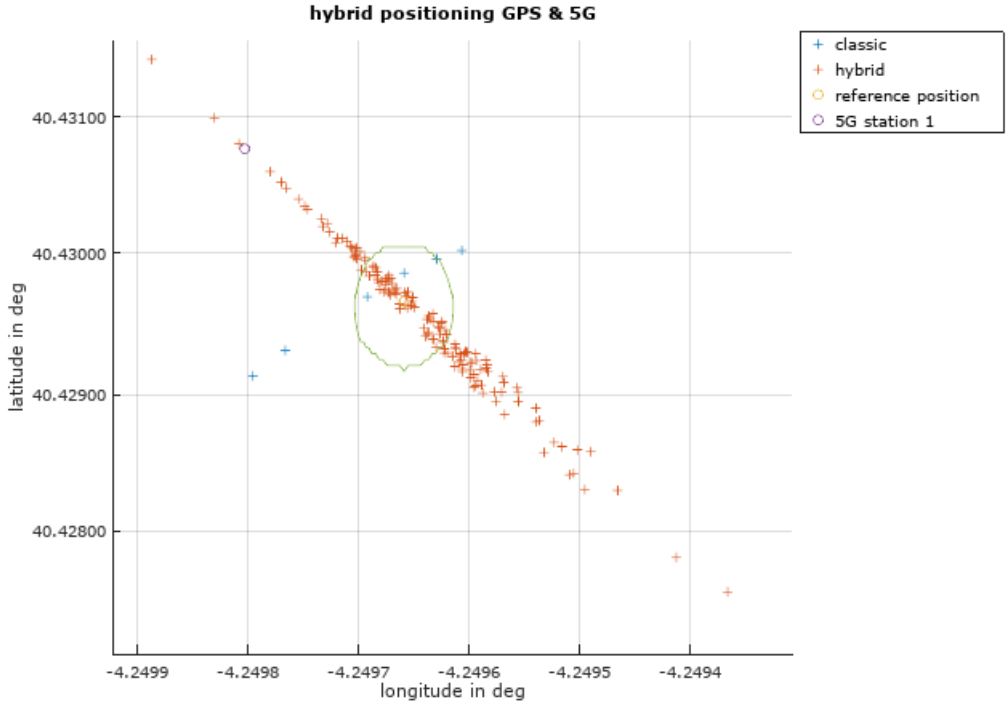

It can be concluded that in urban environment the use of hybridized solution provides better availability compared to the classic solution. Nevertheless, due to a lack of satellite (60deg of masking angle) the accuracy of the hybridized solution is not better than the classic one. It can also be seen that mixed solution are provided on the other side of the 5G station. Indeed the 5G measurements are line equation and every solution (even behind the 5G station) complies with the line equation. A mathematical constraint of half-line equation (directional information) can be applied for further studies.

The above figure is obtained from GPS only observations and it can be supposed that simulation with observations from more satellites can provide solutions closer to the semi-urban environment.

4.3.7 Conclusions

In the case of 5G stations close to the user (under 20m), the solution with best accuracy seems to be the “5G only” solution. In case the receiver is not capable of acquisition of two 5G stations in urban environment, hybridization of the GNSS solution with 5G data improve the availability of the solution.

In semi-urban environment, hybridization improves the accuracy of the classic GNSS solution but the “5G only” solution is still the best solution in term of accuracy.

In rural environment (5G station farther than 500m), hybridized and 5G solutions do not bring benefits to accuracy.

It can be conclude from previous analyses that the rural environment needs to be excluded from the real test campaign in order to get the best results from the mixed solution. Nevertheless the critical configuration (elevation mask and 5G stations distance) when the 5G observations degrades the solution would be interesting to assess.

5 Test bed

5.1 Architecture

5.1.1 Overview

The architecture of the test bed is presented in the figure below.

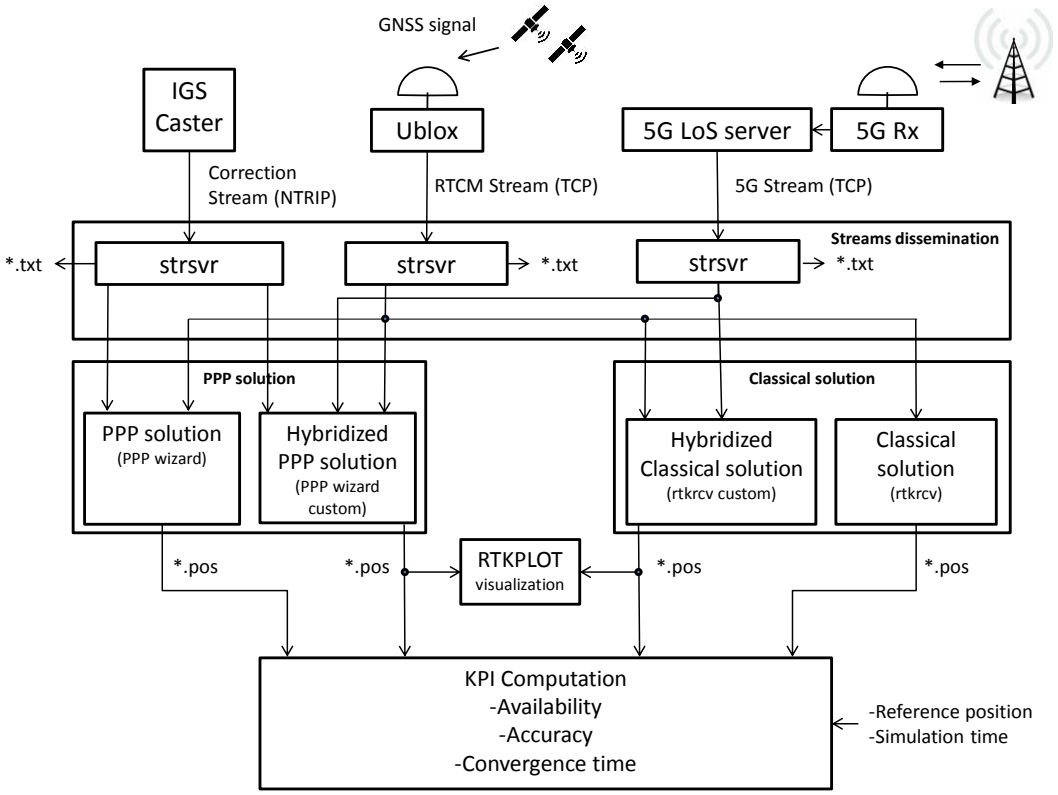

Figure 31: Test bed architecture

5.1.2 Data collection

PPP corrections, GNSS observations and 5G observations comes from different sources and need to be retrieved.

5.1.2.1 PPP corrections from IGS

PPP corrections are retrieved from the IGS caster through a NTRIP connection.

5.1.2.2 GNSS observations from GNSS receiver

The GNSS receiver shall be capable of processing the signals from the new Galileo constellation. Mass-market receivers are not yet compatible with Galileo: the new evaluation kit from ublox will be used instead (EVK-M8T model, see Figure 32 below), which allows to record raw measurements from Galileo, GPS and GLONASS for post processing. In order to fit the most to the capabilities of current smartphones, the receiver will be single-frequency only, and a simple antenna patch will be connected to it. Dual-frequency receivers are preferable because they can remove errors due to ionosphere delays, but these errors are also removed with the PPP method (using the corrections provided by reference networks) and without using a costly receiver.

Figure 32: GNSS receiver

The GNSS receiver can also be a smartphone (Samsung Galaxy S8). The smartphone is capable of providing RTCM messages for the GPS constellation thanks to the CNES application “RTCM converter”. The application allows the use of GPS only.

Both GNSS observations are sent through NTRIP connection (safe TCP connection).

5.1.2.3 5G observations from mmWave subsystem

The full capabilities of mmWave positioning system will be investigated via computer simulations. The system used to demonstrate the mmWave positioning system consists of mmWave radio unit and the laptop to run the positioning algorithm. The mmWave radio is mmWave backhaul radio unit (BRU) used in the EU side radio access network for 5G radio link. As described in deliverable [D2.1] the mmWave system consists:

- mmWave backhaul radio unit (BRU) with support for beamforming. BRU includes mmWave air interface (AI0) and L1/L2 interface (I1) for IP traffic
- multi-RAT radio unit operates as traffic aggregator/multiplexer from the wireless backhaul to other radio technologies.

Further details of the output of the BRU is defined in: [D3.1], [D3.5], [D3.6]; as well as the software components and algorithms in: [D3.2], [D3.3], [D3.4].

A laptop is interfaced via Ethernet/Wifi to the BRU as well as to another computer running the mixed algorithm.

In case the 5G observations cannot be provided by RF hardware, the observations are simulated as close to the real HW as possible and sent with a server.

5.1.3 Data dissemination

5.1.3.1 PPP corrections and 5G observations

The PPP corrections and 5G observations are retrieved and made available via to the TPZ server thanks to a NTRIP connection.

5.1.3.2 GNSS observations

The GNSS observations are retrieved from the receiver via USB with u-center (see **Erreur ! Source du renvoi introuvable.**) and made available via the TAS server thanks to a NTRIP connection.

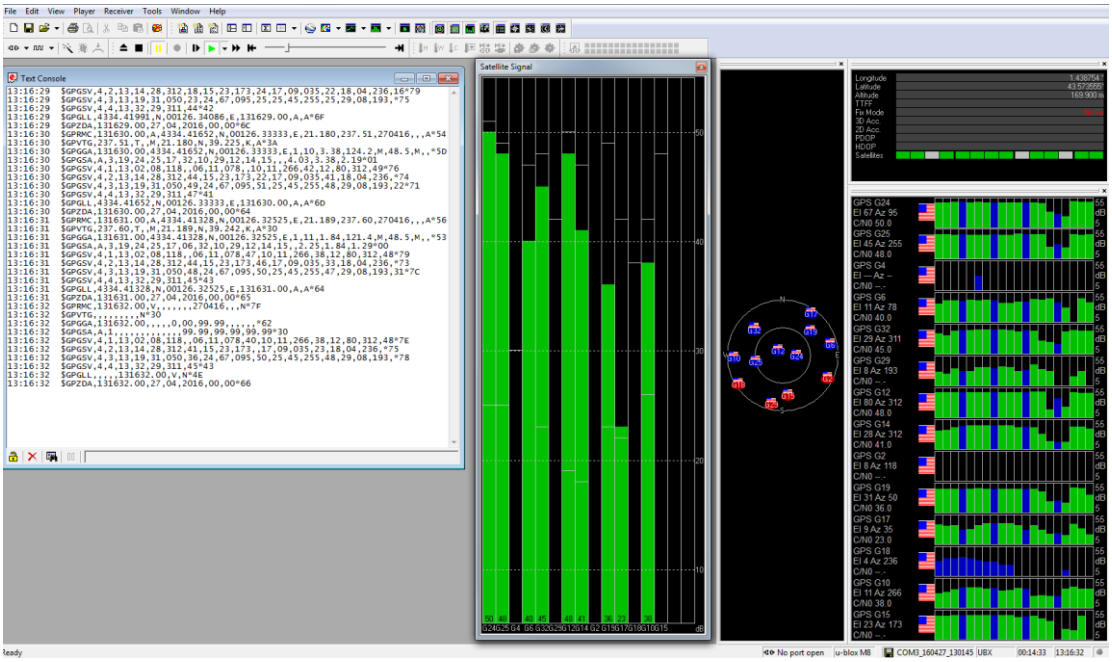

Figure 33: u-center interface

5.1.4 Positioning subsystem

5.1.4.1 PPP solution and hybridization

The PPP solution and hybridized PPP solution is done with the software PPPwizard. The software is installed in the TAS laptop and is fed with GNSS observations from TAS server, PPP corrections and 5G observations from TPZ server.

Both PPP only and hybridized PPP solutions are provided by TAS under the same format as the RTKLIB solution (*.pos). The hybridized solution is also streamed via NTRIP connection for real time visualisation under RTKPLOT (see Figure 34: rtklib interface).

5.1.4.2 Classical solution and hybridization

The classical solution and hybridized solution is done with the software rtknavi/rtkrcv (windows/Linux). The software is installed in the TPZ laptop and is fed with GNSS observations from TAS server 5G observations from TPZ server.

Both classical only and hybridized solutions are provided by TPZ under the format defined by RTKLIB (*.pos). The hybridized solution is also streamed via NTRIP connection for real time visualisation under RTKPLOT.

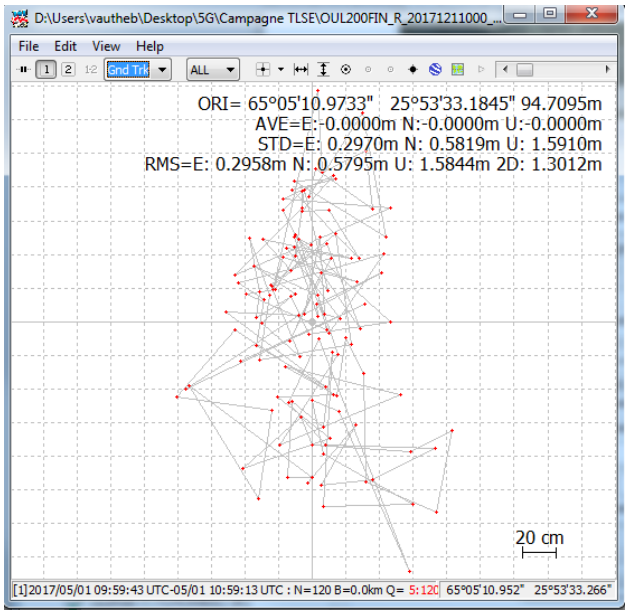

Figure 34: rtklib interface

5.1.5 Post processing subsystem

The KPI (availability, accuracy and convergence time) are computed and plotted with a Matlab file.

5.1.6 Data transfer

The PPP corrections are retrieved from the Internet. Except the PPP corrections, all the streams are exchanged on a local network hosted on a smartphone. Each stream is also recorded to allow the re-running of the observations on real time.

5.2 Test cases

Three types of environment are considered for reflecting ubiquitous positioning: open sky, semi urban and indoor. The GNSS-only and mixed solutions are intended to be tested in the open sky and semi urban environments, but not in indoor because of the lack of satellite signals in this environment. For the mmWave-only solution currently in development, theoretical results will be presented for all three environments.

Positioning system →	mmWave-only	mmWave+GNSS	GNSS-only
Open sky	Theoretical results	✓	✓
Semi urban	Theoretical results	✓	✓

Indoor	Theoretical results	×	×

For each environment, stations at 10, 20 and 50 meters from both the north and the east will be considered as test case. A more precise description of the test cases is provided on the D6.3 document (Integration and system testing phase of satellite scenario).

The tests will be static and conducted in the TAS facilities with simulated 5G observations.

5.3 Expected results

5.3.1 GNSS positioning

For GNSS positioning, the PPP method has its full potential in a clear-sky environment like rural areas. Indeed, a large number of satellites are available and multipath is rare.

In an urban environment, buildings mask satellites and generate multipath. The position given by GNSS may not be accurate enough: that is why a mixed algorithm combining GNSS and 5G measurements is proposed in section 4.

In indoor environment, the use of a positioning solution based on GNSS is not possible since signals are blocked by the building materials.

5.3.2 5G positioning

From the 5G only –case, the main expected results as research outcome will be first, the algorithm design and verification via simulation as well as performance comparison against analytical lower bounds, and second, the verification via performing the simulation based on real life measurements with the pre-commercial 5G mmWave PoC platform. The results are reported on a high quality peer-reviewed conference publications, namely targeting to European Conference on Networks and Communications (EUCNC) and European Signal Processing Conference (Eusipco), In addition to the conference articles, the results will be collected and reported on the journal article, .e.g. IEEE Transactions or IEEE Magazine articles.

Outcome targeting to the industrial community, the main expected results is the showcase of the algorithm on a PoC demonstration platform. Namely, a fully functional algorithm accounting the different levels of information available, and functionality referring to the implementation level of the algorithm so that it will interoperate with server running 5G-GNSS mixed algorithm. Thus, it will be possible to verify and compare the results in different real life scenarios.

5.3.3 Mixed algorithm

The expected results of the mixed positioning solution are strongly related to the KPI calculated in section §4.3.

It has to be noted that $\sigma_{5G}$is a variance that depends on the position. The closer the receiver is to the 5G antenna, the lower the variance. This means that depending on the situation, σ_{5G}can be smaller or greater than σ_{UERE} The expected result is therefore:

- In a urban configuration, where the 5G antennas are close to the user, the positioning thanks to 5G will significantly improve the KPI
- In a country-side environment where antennas are far away and satellites are easily tracked, the best solution shall not include 5G equations

- Somewhere in the middle there shall be an environment where the cooperation between both techniques is possible. The satellites will provide good positioning and the 5G can cut out multipath.

6 Conclusion

This report has led to the description of the GNSS precise positioning techniques and to the selection of the one which is the most suitable regarding positioning use cases, It has also explained the concept of mmWave positioning and has defined an algorithm mixing information from GNSS and 5G to provide a robust and precise positioning in urban environment. Lastly, it has described a preliminary architecture of the test bed, listed the test cases and the expected results.

All these inputs will be used to develop and implement in the following months the positioning test bed that will be demonstrated in the University of Oulu.

References

[1] Tobías, Guillermo, Calle, J. David, Navarro, Pedro, Rodríguez, Irma, Rodríguez, Daniel, "Real-Time PPP with Galileo, Paving the Way to European High Accuracy Positioning," *Proceedings of the 27th International Technical Meeting of The Satellite Division of the Institute of Navigation (ION GNSS+ 2014)*, Tampa, Florida, September 2014, pp. 2354-2362.

[2] Simon Banville, Frank Van Diggelen, “Innovation : Precise positioning using raw GPS measurements from Android smartphones”, *GPS World*, nov 2016

[3] *Osseiran, A.; Boccardi, F.; Braun, V.; Kusume, K.; Marsch, P.; Maternia, M.; Queseth, O.; Schellmann, M.; Schotten, H. (2014-05-01).* "Scenarios for 5G mobile and wireless communications: the vision of the METIS project"*. IEEE Communications Magazine*

[4] M. Elsobeiey; A. El-Rabbany. “Convergence Time Improvement of Precise Point Positioning”. *Geodetic Applications in Various Situations, 5249*

[P1] M. El-Nozahi, E. Sanchez-Sinencio and K. Entesari, "A Millimeter-Wave (23–32 GHz) Wideband BiCMOS Low-Noise Amplifier," *IEEE Journal of Solid-State Circuits*, vol. 45, no. 2, pp. 289-299, Feb. 2010.

[P2] J. G. Andrews et al., “What will 5G be?,” IEEE J. Sel. Areas Commun., vol. 32, no. 6, pp. 1065–1082, 2014.

[P3] M. Mueck et al., “5G CHAMPION - Rolling out 5G in 2018,” IEEE Globecom Workshops, 2016, pp. 1–6.

[P4] S. M. Razavizadeh, M. Ahn, and I. Lee, “Three-dimensional beamforming: A new enabling technology for 5G wireless networks,” *IEEE Signal Process. Mag.*, vol. 31, no. 6, pp. 94–101, 2014.

[P5] T. S. Rappaport, S. Sun, R. Mayzus, H. Zhao, Y. Azar, K. Wang, G. N.Wong, J. K. Schulz, M. Samimi, and F. Gutierrez, “ Millimeter WaveMobile Communications for 5G Cellular: It Will Work!,” *IEEE Access*, vol. 1, pp. 335-349, 2013.

[P6] G. Destino, J. Saloranta, and M. Juntti, “Robust 3D MIMO-OFDM Channel Estimation with Hybrid Analog-Digital Architecture,“ *2016 24th European Signal Processing Conference (EUSIPCO)*, Budapest, 2016, pp. 1990-1994.

[P7] J. Saloranta and G. Destino, “On the Utilization of MIMO-OFDM Channel Sparsity for Accurate Positioning,” 2016 24th European Signal Processing Conference (EUSIPCO), Budapest, 2016, pp. 748-752.

[P8] C. B. Do and S. Batzoglou, “What is the expectation maximization algorithm?,” *Nat. Biotechnol.*, vol. 26, no. 8, pp. 897–899, Aug. 2008.

[P9] G. Destino, M. Juntti, and S. Nagaraj, “Leveraging sparsity into massive mimo channel estimation with the adaptive-lasso,” Proc. IEEE Global Signal Process. Conf., Dec. 2015.

[P10] A. Shahmansoori, G. E. Garcia, G. Destino, G. Seco-Granados, and H. Wymeersch, “5G Position and Orientation Estimation through Millimeter Wave MIMO,” Proc. IEEE Global Commun. Conf. Workshops, Dec. 2015, pp. 1–6.

[P11] Jani Saloranta, and Giuseppe Destino, “Reconfiguration of 5G Radio Interface for Positioning and Communication,” Proc. European Signal Processing Conference

(EUSIPCO), Aug 2017.

[P12] Jani Saloranta, Giuseppe Destino, and Henk Wymeersch, “Comparison of Different Beamtraining Strategies from a Rate-Positioning Trade-Off Perspective,” European Conference on Networks and Communications (EuCNC), Jun 2017.

[P13] Giuseppe Destino, Jani Saloranta, Henk Wymeersch, and Gonzalo Seco-Granados, “Impact of Imperfect Beam Alignment on the Rate-Positioning Trade-Off,” IEEE Wireless Communications and Networking Conference (WCNC), 2018.

[P14.] Praneeth Susarla, Jani Saloranta, Giuseppe Destino, Olli Kursu, Marko Sonkki, Marko E. Leinonen, Aarno Pärssinen, “Smart-RF for mmWave MIMO Beamforming”, IEEE International Symposium on Personal, Indoor and Mobile Radio Communications (PIMRC) 2018, [submitted].

[D2.1] 5GCHAMPION Deliverable D2.1, “5GCHAMPION Architecture, API- and interface document”, Mar 2017.

[D3.1] 5GCHAMPION Deliverable D3.1, “Front-end design”, Dec 2016.

[D3.2] 5GCHAMPION Deliverable D3.2, “Electronically Reconfigurable Antenna Arrays for Backhauling & Fronthauling”, Oct 2017.

[D3.3] 5GCHAMPION Deliverable D3.3, “Beamforming antennas and front-end integration”, Jan 2018.

[D3.4] 5GCHAMPION Deliverable D3.4, “Algorithms for backhauling & fronthauling”, May 2017.

[D3.5] 5GCHAMPION Deliverable D3.5, “mmWave backhauling & fronthauling platform”, May 2017.

[D3.6] 5GCHAMPION Deliverable D3.6, “mmWave backhauling & front hauling implementation”, Apr 2018.

[D6.1] 5GCHAMPION Deliverable D6.1, “Access and backhaul: Integration and system testing”, Jul 2017.